The Impact of Allosteric Modulators on The Orthosteric and Allosteric Binding Pockets

by

Chih-Jung Chen

B.S in Pharmacy, Kaohsiung Medical University, 2018

Submitted to the Graduate Faculty of the

School of Pharmacy in partial fulfillment

of the requirements for the degree of

Master of Science

University of Pittsburgh

2022

UNIVERSITY OF PITTSBURGH

SCHOOL OF PHARMACY

This thesis/dissertation was presented

by

Chih-Jung Chen

It was defended on

March 23, 2022

and approved by

Xiang-Qun (Sean) Xie, Ph.D., EMBA, Professor, Department of Pharmaceutical Sciences

Levent Kirisci, Ph.D., Professor, Department of Pharmaceutical Sciences

Junmei Wang, Ph.D., Associate Professor, Department of Pharmaceutical Sciences

Zhiwei Feng, Ph.D., Assistant Professor, Department of Pharmaceutical Sciences

Thesis Advisor/Dissertation Director:
Zhiwei Feng, Ph.D., Assistant Professor, Department of Pharmaceutical Sciences

The Impact of Allosteric Modulators on The Orthosteric and Allosteric Binding Pockets

Chih-Jung Chen, B.S.

University of Pittsburgh, 2022

ABSTRACT

Allosteric modulators (AM) that bind allosteric sites can exhibit greater selectivity than the orthosteric ligands and can either enhance agonist-induced receptor activity (termed positive allosteric modulator, or PAM), inhibit agonist-induced activity (negative AM, or NAM), or have no effect on activity (silent AM, or SAM). Until now, it is not clear what the exact effects of AMs are on the orthosteric active site or the allosteric binding pocket(s). In the present work, we collected both the 3D structures of receptor-orthosteric ligand and receptor-orthosteric ligand-AM complexes of a specific target protein. Using our novel algorithm toolset-Molecular Complex Characterizing System (MCCS), we were able to quantify the key residues in both the orthosteric and allosteric binding sites along with potential changes of the binding pockets. After analyzing 21 pairs of 3D crystal or cryo-EM complexes, including 4 pairs of GPCRs, 5 pairs of ion channels, 11 pairs of enzymes, and 1 pair of transcription factors, we found that the binding of AMs had little impact on both the orthosteric- and allosteric- binding pockets. In return, given the accurately predicted allosteric binding pocket(s) on a drug target of medicinal interest, we can confidently conduct the virtual screening or lead optimization without concern that the huge conformational change of the pocket could lead to the low accuracy of virtual screening.

Keywords: Allosteric modulator, MCCS, drug discovery

Table of Contents

Preface x

1.0 INTRODUCTION 1

1.1 Allostery 1

1.2 Allosteric Site 3

1.3 Allosteric Modulators 4

1.4 Research Regarding Allostery 6

1.5 Purpose 9

2.0 METHODS AND MATERIALS 11

2.1 Protein−Ligand(s) Complexes 11

2.2 Molecular Complex Characterizing System (MCCS) 11

2.3 Alignment of the Structures and Calculation of RMSD 14

2.4 In-Silico Site-Mutagenesis 14

2.5 Molecular Dynamics (MD) Simulation 14

3.0 RESULTS AND DISCUSSION 16

3.1 Innovation and Application of MCCS 16

3.2 Stabilization of Both GPCRs and Orthosteric Ligands by AMs 17

3.3 Stable Conformations and Interaction of the Enzymes-Orthosteric Ligand by AMs 23

3.4 Stability in Ion Channels and Transcription Factor 32

3.5 Comparison of Orthosteric and Allosteric Binding Sites Between the 21 Pairs X-Ray Crystal or Cryo-EM Complexes 40

3.6 Molecular Dynamics Simulation Studies..... 44

4.0 CONCLUSION 52

Bibliography 54

List of Tables

Table 1. AM drugs approved by US FDA..... 8

Table 2. Sixteen pairs of complexes consisted of either agonist with PAM or antagonist with NAM. 42

Table 3. Five pairs of complexes comprised of either agonist with NAM or antagonist with PAM. 44

List of Figures

Figure 1. Articles regarding "allosteric" in SciFinder^n from 2000 to 2021. 7

Figure 2. The workflow of MCCS. 13

Figure 3. The comparison of the complex of M2-iperoxo(agonist) with/without the binding of the positive allosteric modulator (PAM)-LY2119620..... 18

Figure 4. The comparison of the complex of β2-carazolol(antagonist) with/without the binding of the negative allosteric modulator (NAM)-Cmpd-15. 21

Figure 5. The comparison of the complex of MEK1-ATP-γS(agonist) with/without the binding of the negative allosteric modulator (NAM)-Compound-1. 26

Figure 6. The comparison of the complex of GK-α-D-glucopyranose(agonist) with/without the binding of the positive allosteric modulator (PAM)-TAFMT. 29

Figure 7. The comparison of the complex of NMDARs-glycine/glutamate with/without the binding of PAM-GNE3419. 35

Figure 8. The comparison of the complex of NMDARs-glycine/glutamate with/without the binding of NAM-compound 6. 36

Figure 9. The comparison of the complex of AR-testosterone (TES) with/without the binding of negative allosteric modulator (NAM)- 4-(2,3-dihydro-1H-perimidin-2-yl) benzene-1,2-diol. 38

Figure 10. The detailed energy contributions of important binding residues in the orthosteric pocket of AR. 39

Figure 11. RMSD of PDB 4MQT-4MQS structures during MD simulation course. 46

Figure 12. MD simulation studies of PDB 4MQT-4MQS structures. 48

Figure 13. RMSD of PDB 5X7D-2RH1 structures during MD simulation course. 49

Figure 14. MD simulation studies of PDB 5X7D-2RH1 structures. 51

Preface

I sincerely appreciate my advisor Dr. Zhiwei Feng. During my Master's program, he not only taught us many computational techniques but also gave us many suggestions for research and life. We have group meetings once a week, in which we report the progress and discuss the problem of our projects. I can also contact him easily to discuss some problems or ideas for my ongoing projects. He encourages us to show ourselves in front of people via oral presentation and gives me many suggestions for slides and the talk. Importantly, he leads us to think creatively and independently when we work on projects and write manuscripts, which will benefit me a lot in my future research.

I would like to express my gratitude to Dr. Xiangqun Xie. He is the director of the PSP track, CCGS center, and the CB2 joint project. I learn many research aspects and techniques in Computational System Pharmacology Course and Pharmacometrics Course. The CCGS center gives us many opportunities to give oral presentations and discuss our projects with people from similar research fields. The CB2 joint project gives us opportunities to collaborate with professionals from diverse research areas.

Meanwhile, I want to thank my committee member, Dr. Junmei Wang and Dr. Levent Kirisci. Dr. Junmei Wang is a professor in Computational System Pharmacology Course, Pharmacometrics Course, and Foundation in Pharmaceutical Sciences Course and a faculty member at the CCGS center. I learn a lot from his classes and his attitude as well as his enthusiasm for research. Dr. Levent Kirisci is a professor in Statistical Methods Course. I learn a lot from his classes which gives me the statistical knowledge I need in the research.

I also want to express my sincere acknowledgment to all the team members at Dr. Xiangqun Xie's lab and CCGS center. Especially, I want to thank Maozi Chen who is the IT scientist in our lab. He taught me to step by step to apply MCCS, led me to think about how to write the bash code to conduct MCCS to deal with amounts of data, and provide me with a lot of technical support. I also want to thank Dr. Terence McGuire and Dr. Jaden Jun who are the professors and team leaders at our CCGS center and R01 CB2 Joint Project. They give me suggestions for my projects with perspective from their research fields, and I learn the research knowledge and experience from them. At the same time, I want to thank the support and assistance from my labmates and peers during my two-year studies.

Last, I want to thank my parents for their full support during my Master's program, and my friends who support and accompany me during the remote study in the first year.

I offer my warmest regards and sincere blessings to all of those who help me during my two-year studies in any respect.

1.0 INTRODUCTION

1.1 Allostery

Allostery, also called allosteric regulation, is a process or phenomenon where a macromolecule (mostly protein) transmits the effect caused by an allosteric interaction at an allosteric binding site which is spatially and topographically remote from the active site and leading to the regulation of the macromolecule activity.[1-3] Allosteric signals are transmitted from allosteric binding sites across the macromolecules to the active site, and the signaling pathway includes atomic fluctuations, residues networks, or domain movements.[2, 4-6] Allosteric interactions can be noncovalent contacts (ions, small molecules, peptides, nucleic acids, lipids, and proteins),[2, 7-12] covalent modifications (phosphorylation, point mutations, and disulfide trapping),[2, 13-17] environmental fluctuations (pH, temperature, and ionic strength),[18] and light absorption.[2, 19-21]

Compared to the orthosteric ligands, allosteric modulators (AMs) have the following benefits. Since the proteins in the same family are coded by homologous genes, their orthosteric binding sites are always highly conserved, especially in protein kinases and G-protein coupled receptors (GPCRs). In contrast, allosteric sites are often less conserved since the allosteric effects can arise in varied regions on proteins other than active sites.[2, 22, 23] Therefore, AMs possess better selectivity between subtypes and thus have fewer side effects than orthosteric ligands.[24-26] Even if the binding affinities of an AM are the same for different subtypes in a protein family, it can still deploy selectivity since the cooperation between orthosteric and allosteric sites may be different to some extent.[27, 28] In addition, there is an “effect ceiling” for AMs since they only

cause an effect when an orthosteric ligand is binding to the protein, and, they only regulate rather than eliminating or activating the proteins, which makes them safer than orthosteric ligands.[2, 14, 29] If a target protein is activated by special stimuli, such as divalent cations, light, and portions, it is hard to design a drug to mimic the orthosteric effect. However, AMs may be able to regulate this type of protein.[30] Besides, AMs have the potential to fine-tune a specific tissue with indirect allosteric effects on a protein involved in lateral protein interaction, where several proteins co-expressed in the same cell and associate with each other to form homomers or heteromers to generate physiological function.[31, 32]

Nonetheless, there are some disadvantages and challenges for developing novel AMs. Some of the allosteric pocket structures are flat and non-tractable, resulting in less effective AMs.[33] For instance, the binding affinities of many AMs for GPCRs only exist micromolar range.[34] In addition, AMs for non-conserved allosteric sites may easily arouse drug resistance by point mutation, especially in the system with rapid genetic mutation and selection, such as anti-viral, anti-bacterial, and anti-cancer therapeutic areas.[35, 36] Moreover, the low evolutionary conservation of allosteric sites may lead to different pockets between species. Therefore, the animal model experiments may mismatch the results in the human body, which hinders the development of allosteric drugs.[33, 34] Besides, although there are many possible allosteric pockets on a protein surface, discovering a highly effective allosteric site is still a challenge.[37-39] Furthermore, unlike the design of orthosteric compounds that can refer to endogenous substrates, the development of AMs may need to start from creating a new scaffold.[40]

1.2 Allosteric Site

When residues in allosteric binding sites interact with AMs, they generate the allosteric signal and can modulate the protein activity as well as the binding affinity of orthosteric ligands via remote control. They are more nonconservative than orthosteric binding sites. Calculated from homologous sequence alignments with 58 enzymes of various species, the average conservation score of residues in allosteric pockets is 0.58, while that of orthosteric site residues is 0.94.[23]

Allosteric binding pockets are prone to be more hydrophobic than orthosteric pockets. Compared to orthosteric binding pockets, there are more hydrophobic residues in allosteric sites, such as leucine, valine, isoleucine, phenylalanine, and proline. The few charged residues in allosteric binding sites play important roles in specific ligand interactions and facilitate ligand binding. Specifically, when the polar residues in allosteric pockets are replaced by hydrophobic residues, the binding affinity of AMs decrease. Moreover, higher hydrophobicity allows allosteric binding pockets to be more tolerant for mutations since it is easier for hydrophobic residues to be substituted by a residue with a similar size compared to charged residues which may also involve in a specific polar network.[23, 41, 42] In addition, the interfaces of proteins or subunits coupling are common to be allosteric binding sites,[43] and they are generally more hydrophobic.[44-46]

On the other hand, orthosteric binding sites are comprised of more abundant polar residues than allosteric pockets, such as aspartic acid, asparagine, glutamic acid, and histidine. Amino acids in possession of hydroxyl groups, such as threonine, serine, and tyrosine, are also more enriched in orthosteric sites than in allosteric pockets. With more hydrophilic residues, there are higher opportunities within orthosteric pockets to form specific connections with ligands, such as hydrogen bonds networks, to promote ligand binding.[23, 41, 42]

Moreover, orthosteric binding sites are more common to form covalent bonds with orthosteric ligands, such as phosphorylation, while allosteric pockets seldom covalently connect with AMs. Residues with hydroxyl groups which are more abundant in orthosteric pockets than allosteric sites can form covalent bonds with ligands.[2, 13, 47, 48]

1.3 Allosteric Modulators

Allosteric signal propagation pathways are pre-existing in proteins and activated by the binding of AMs. When an AM bind to the target protein, they induce a specific allosteric pathway among the ensemble of pre-existing pathways and do not create a new conformation of the protein.[49, 50]

AMs bind to allosteric sites different from orthosteric binding sites, and thus, they are non-competitive effectors that do not compete with endogenous substrates or orthosteric ligands. Based on the pharmacological features, AMs can be divided into three categories, positive allosteric modulator (PAM), negative allosteric modulator (NAM), and silent allosteric modulator (SAM). PAMs increase the activation of agonists of a receptor by raising their affinity or efficacy. They may also promote the G protein coupling in GPCRs. NAMs reduce the affinity or the efficacy of agonists to decrease the activation of agonists or stabilize the inactive state of the receptor that is bound with antagonists. SAMs have no impact on the activity of orthosteric ligands, but they occupy the allosteric binding sites, resulting in the blocking of the allosteric activities from PAM and NAM.[2, 51]

Allosteric binding sites of PAMs and NAMs on a specific protein can be at the same pocket or different sites. The chemical features of PAMs and NAMs binding to the same binding site may

only have subtle differences, such as a change of a single atom or a small group. Detailed interaction between AMs and the protein may determine the pharmacological effects caused by AMs. Atoms in AMs can be divided into two parts: anchor and driver. The anchor atoms form favorable interactions with the protein, which do not alter during the transition of protein conformations from active to inactive states. The driver part interacts with protein and can either become attractive "pulling" atoms or repulsive "pushing" atoms to stabilize/destabilize the allosteric active/inactive conformation. For example, the attractive interaction between the allosteric pocket and the driver atoms may pull the inactive conformations to transform into active states. Therefore, subtle modification on the driver atoms of AMs may lead to opposite pharmacological effects.[50, 52]

AMs have some common structural and physicochemical properties. Smith et al.[44] collect and analyze information of compounds from ASD (http://mdl.shsmu.edu.cn/ASD/) and ChEMBL (https://www.ebi.ac.uk/chembl/) to investigate the features of AMs and compare them with orthosteric ligands. They find that there are more aromatic atoms and fewer saturated bonds on heavy atoms in AMs, leading to the fewer number of rotatable single bonds in AMs and thus resulting in more rigid and constrained structures of AMs, although allosteric binding sites often undergo conformational change when AMs bind. Wang et al.[53] and Van Westen et al.[35] report similar results. The former states that AMs have significantly fewer rotatable bonds compared with drug molecules from DrugBank. The latter reveals that for transmembrane proteins, AMs possess more sp2 hybridized carbons, fewer sp3 hybridized carbons, and more aromatic atoms compared to orthosteric ligands. All in all, relatively rigid AMs bind to allosteric binding sites and induce a change in protein flexibility to accommodate AMs.[44] Furthermore, although allosteric binding sites are inclined to be hydrophobic, AMs may not be more hydrophobic than orthosteric ligands.

Smith et al. conduct large-scale statistics and find that there is no significant difference regarding hydrophobicity between AMs and orthosteric ligands.[44]

1.4 Research Regarding Allostery

In the past two decades, studies and publications regarding allosteric mechanisms, pockets and AMs have grown at fast pace. **Figure 1** shows the related articles in SciFinder^n climbing from 721 in 2000 to 2153 in 2020. Importantly, 56 AM drugs have been approved by the US FDA, in which there are 4 for G-protein coupled receptors (GPCRs),[54-57] 40 for ion channels,[58-83] and 13 for enzymes[84-95] (**Table 1**). For example, the oldest approved AM in the US is chlordiazepoxide, a benzodiazepine drug approved in 1960 for alcohol withdrawal syndrome and anxiety.[96] Chlordiazepoxide is a PAM for GABA-$_A$ receptor that can increase the frequency of GABA-induced chloride channel openings and enhance the binding affinity of GABA in its orthosteric binding site.[97, 98] Subsequently, several benzodiazepines came on the market in the mid- and late-twentieth-century, and the success of benzodiazepines in clinical practice caught the eye of the researchers focused on allosteric drug discovery.[60-63, 99] In 1998, the first enzyme AM, rifapentine, was approved by the FDA. It is a NAM for bacterial RNA polymerase (RNAP) for the treatment of tuberculosis infection.[89] In 2004, the first GPCR AM, cinacalcet, appeared on the market for the treatment of secondary hyperparathyroidism and parathyroid carcinoma.[100-104] Cinacalcet is a PAM of calcium-sensing receptor (CaSR) and can increase the sensitivity of the calcium-sensing receptor for activation by extracellular calcium.[54] The blossoming of AMs in the market makes the development of allosteric drugs an increasingly hot research area.

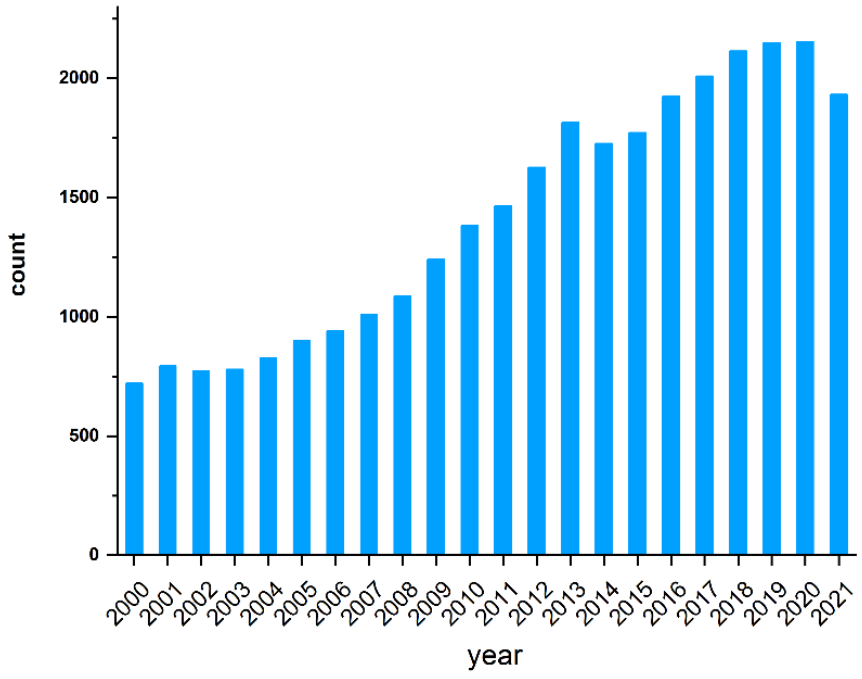

Figure 1. Articles regarding "allosteric" in SciFinder" from 2000 to 2021.

With transmission electron cryo-microscopy (cryo-EM), X-ray crystallography, and other innovative technologies, more and more 3D crystal structures complexed with AMs in high resolution have been released. There are 6,772 complexes containing allosteric agents in the Protein Data Bank (https://www.rcsb.org/).[105] The Allosteric database (http://mdl.shsmu.edu.cn/ASD/) cumulates 82,070 molecules with allosteric modulation features and 538 drugs from preclinical phases to approved status.[106] The high quality of 3D complexes of the protein with modulator allows structural biologists to investigate the binding pocket(s) of receptors, the binding poses of orthosteric ligands and AM(s), and the potential conformational changes of the target protein. For example, Liu *et* al. reported two crystal structures that included (1) β2 adrenoceptor (ADRB2) binding with orthosteric antagonist carazolol and (2) the complex of ADRB2-carazolol-Cmpd-15(NAM compound 15). Their studies unveiled the important residues involved in the interactions between Cmpd-15 and ADRB2, the conformational changes caused by the binding of modulator that stabilized the inactive inward conformation of TM6, and

the prevention of coupling to Gs protein caused by the steric clash with Cmpd-15.[107] In addition, the high-quality 3D structures of protein complexed with AMs improves the accuracy of computational experiments and thus facilitate in-silico drug discovery.

Table 1. AM drugs approved by US FDA

GPCRs	**Enzymes**			
Cinacalcet, ticagrelor, Maraviroc, plerixafor	carglumic acid, trametinib, sirolimus, enasidenib, rilpivirine, rifapentine, cobimetinib, Etravirine, Temsirolimus, Thrombomodulin α, Trametinib, Trastuzumab, Pertuzumab			
Ion channels				
GABA-A receptors	**AMPA Receptors**	**Calcium Channels**	**Sodium Channels**	**Others**
Lorazepam, Flurazepam, Ketazolam, Clonazepam, Cyclothiazide, Diazepam, Triazolam, Alprazolam, Eszopiclone, Topiramate, Chlordiazepoxide, Clobazam, Estazolam, Midazolam, Oxazepam, Quazepam, Remimazolam, Temazepam, Zolpidem, Zaleplon, Zopiclone, Eszopiclone, Etomidate, Propofol, Sevoflurane	Piracetam, Aniracetam, Perampanel	Diltiazem, Verapamil, Isradipine, Nifedipine, Lomerizine, Ziconotide, Pregabalin	Pirmenol, Carbamazepine, Lamotrigine	ivermectin

1.5 Purpose

Dedicated to the development of modulators for GPCRs,[108-112] our lab previously compared and analyzed the existing computational methods for detecting the allosteric sites and designing AMs in our review paper.[113] We compared six approaches for the prediction of the allosteric binding sites, including sequence-based approaches, structure-based methods, conformational dynamics-based approaches, normal model analysis-based approaches, the combination of conformational dynamics-based and NMA-based approaches, and other allosteric-related approaches. For designing the drug candidates, we classified the strategies into three categories, including pharmacophore models, structure-based virtual screening, and molecular dynamics simulation. We delineated every method with a detailed introduction, tools, advantages, challenges, and examples of application study in the article.[113] Recently, to deeply investigate the AMs of GPCRs, we collected the available 3D structures of the class A GPCRs with effective interactions between modulator and receptor, found 7 allosteric binding pockets/regions at GPCRs, and analyzed the binding characterization of allosteric binding pockets. In addition, we further predicted the allosteric binding sites at the CB2 receptor as well as the detailed interaction between CB2 and AMs, which will benefit the development of CB2 allosteric drugs.[114] In addition, we recently developed a novel algorithm tool-set, Molecular Complex Characterizing System (MCCS), which can compute the residue energy contribution to quantify the binding features or pattern of protein-ligand complexes.[115]

In this study, we first collected four-pair complexes in GPCRs, eleven pairs in enzymes, one pair in transcription factors, and five-pairs in ion channels into our dataset. All these targets play important roles in the nervous system. For example, β2 adrenergic receptor belongs to sympathetic nervous system,[116, 117] glucokinase gets involved in the neuronal glucose-sensing

mechanism,[118, 119] and ionotropic glutamate receptors, such as AMPA and NMDAR, modulate neuronal excitability with the excitatory neurotransmitter, glutamate.[120-123] Exploiting our innovative technique, MCCS, we investigated whether the binding of a modulator had an impact on the orthosteric ligand binding via systematically comparing the 3D structure of receptor-ligand with and without a modulator, which would highly facilitate the rational design and development of modulator drug candidates.

2.0 METHODS AND MATERIALS

2.1 Protein−Ligand(s) Complexes

The cryo-EM and X-ray crystal structures were collected from the Protein Data Bank (https://www.rcsb.org).[124] Two different complexes of any target protein were used in our work, including the structure of protein coupled with orthosteric ligand and allosteric modulator as well as the structure of protein bound with orthosteric ligand only. The orthosteric ligand in these two kinds of complexes should be the same.

2.2 Molecular Complex Characterizing System (MCCS)

MCCS[115] was applied to prepare the structures and calculate the residue energy contribution. It can analyze the binding recognition between receptors and ligands by calculating the energy contribution of each residue and the corresponding energy terms, such as hydrogen bonding, hydrophobic force, repulsion, etc.

Figure 2 shows the workflow of the MCCS. After we input the PDB structure, Chimera (version 1.15)[125] was first applied to repair the residues with a truncated side chain. To be more specific, Chimera first scanned the entire protein structures and reported the residues with missing parts. Then, a complete side chain of the same residue type replaced the defective side chains with the Dunbrack rotamer library.[126] Next, we split the complex into the ligand and the protein PDB Files. VEGA[127] was applied to both ligand and protein files to add the Vina force field,

Gasteiger charges, and polar hydrogens. Moreover, VEGA would define rotatable bonds for ligand files. The format of the output files was transformed from PDB into PDBQT by VEGA. In addition, PROPKA (version 3.4)[128, 129] was applied to predict the pKa values of ligands and generated a PKA format. If there was any tertiary (3°) amine in the molecules, it would be protonated by MCCS when the predicted pKa value of ligands was higher than or equal to the given pH (7.4 by default). The PDBQT files of protein and ligand(s) together with the PKA file of ligands form the input of the next step in MCCS- scoring and docking with jdock (version 2.2.3c, https://github.com/stcmz/jdock).

As a variant and successor of idock,[130] *jdock* is a docking and scoring program that can predict the binding pose of a compound within a complex and calculate the total binding free energy as well as energy contribution of each residue which involved in the interaction between a ligand and a protein. The binding affinity of a ligand can then be predicted with the calculated total binding free energy.[131, 132]. Adopting the same 5-term scoring function (gauss1, gauss2, repulsion, hydrophobic, and h-bonding) invented by AutoDock Vina,[133, 134] *jdock* can generate a vector of residue free energy from the conformation either predicted by the Monte Carlo-based docking algorithm or determined by X-ray crystallography or cryo-EM. Those energy terms are related to the distance between two interacting atoms and the van der Waals radii of the interacting atoms.

In this study, we applied the scoring function of *jdock* to analyze the binding features of 21 pairs of X-ray crystal and cryo-EM structures, in which the scores of all receptor-ligand atom pairs were directly calculated and summed to form the overall score. The scoring function in *jdock* can generate nine binding recognition vectors for a given receptor-ligand complex, including (1) Gauss (Gauss1+Gauss2), (2) Gauss1, (3) Gauss2, (4) repulsion, (5) steric (Gauss1+Gauss2+repulsion),

(6) hydrogen-bonding, (7) hydrophobic, (8) non-steric (hydrogen-bonding+hydrophobic), and (9) residue energy contribution. More details can be found in our previous publication.[115]

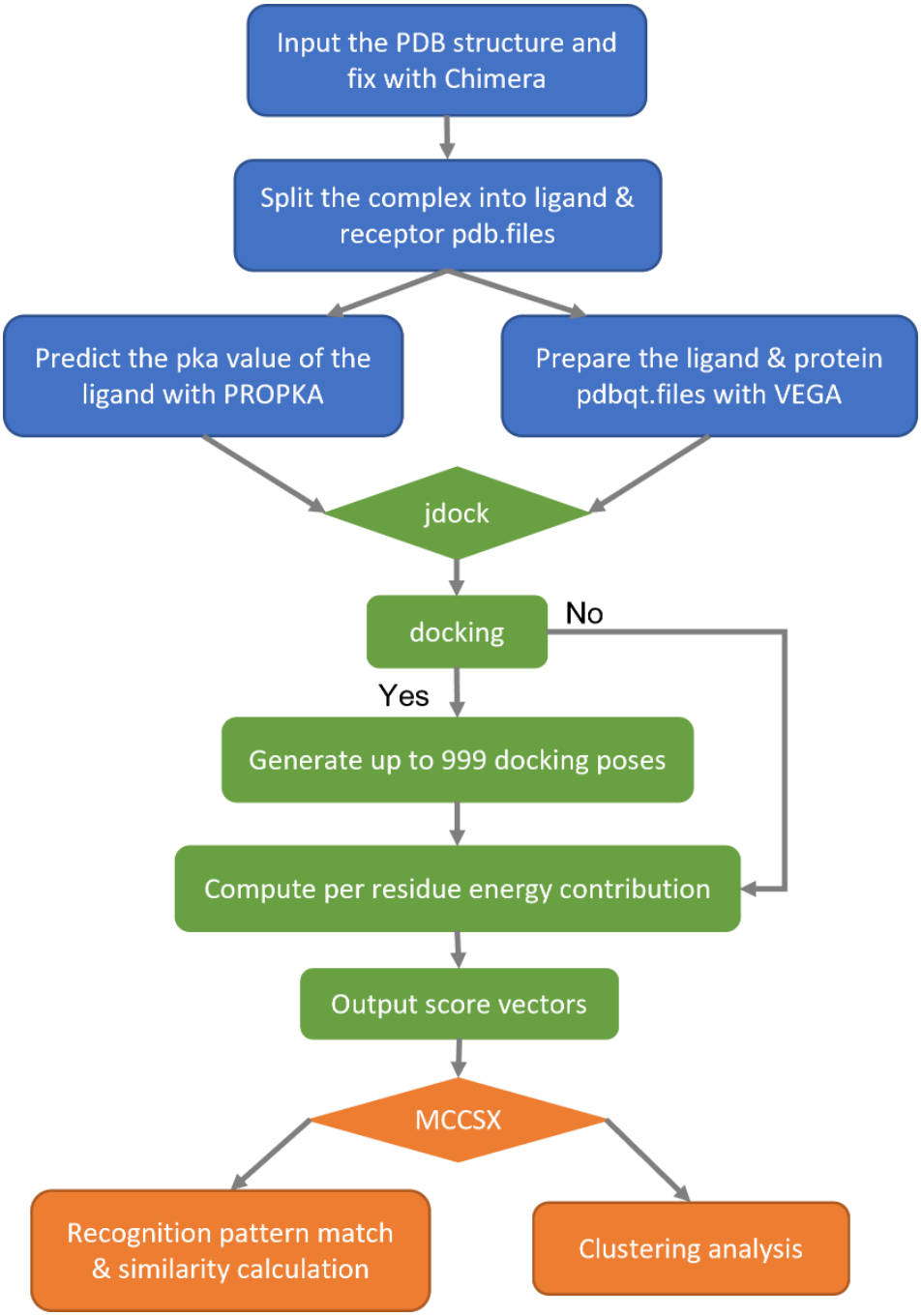

Figure 2. The workflow of MCCS.

The blue portion is the preparation steps. The green part is the performance of jdock. The orange part is the function of MCCSX.

2.3 Alignment of the Structures and Calculation of RMSD

Alignment of the structures within each pair and the root-mean-square deviations (RMSD) value for the protein structure and binding pockets in each pair was calculated by the "align" command in PyMol, which was suitable for the two protein structures with similar sequence. Orthosteric and allosteric binding pockets consisted of residues around the ligands within 8 Å which was the cutoff value for the minimal distance to generate interaction between two atoms and was adopted in the algorithms of jdock in MCCS and Autodock Vina.[133]

2.4 In-Silico Site-Mutagenesis

In-silico site mutagenesis was conducted with the Mutagenesis Wizard in PyMol. The conformation of the mutated residues was selected when the ligands were bound to the receptors.

2.5 Molecular Dynamics (MD) Simulation

Two pairs of complexes, PDB 4MQS-4MQT and PDB 2RH1-5X7D, were set up for MD simulation. Each complex consisted of a receptor and an orthosteric ligand w/o an AM, which were put into a 0.15M NaCl solution with a cubic water box, 300 POPC lipid molecules, and about 20809 TIP3P water molecules[135]. CHARMM-GUI Online Toolkit[136] (https://charmm-gui.org) was applied to add POPC lipids and prepared the bilayer membrane where the membrane protein embedded with the size about 128 Å ×110 Å × 128 Å. The protein was modeled with the

AMBER ff14SB force field[137]. The partial atomic charges of ligands were derived via the semi-empirical with bond charge correction (AM1-BCC) method[138, 139]. The residue topologies for ligands were prepared with the ANTECHAMBER module. The other force field parameters were obtained from GAFF in AMBER16[139].

The MD simulations were conducted with the PMEMD.mpi and PMEMD.cuda modules in the AMBER16[140-142] package. The system was first minimized by several steps to avoid possible steric clashes. Subsequently, each system was gradually heated from 0 K to 300 K during the heating stage and maintained at 300 K during the following equilibrium and production stages with a time step of 2 fs. The constant temperature and pressure ensembles were maintained with a periodic boundary condition. The pressure was set at 1 atm and controlled by the anisotropic (x-, y-, z-) pressure scaling protocol with a pressure relaxation time of 1 ps. The temperature was regulated using Langevin dynamics with a collision frequency of 2 ps^{-1}.[143, 144] The particle mesh Ewald (PME) method[145, 146] was adopted to handle long-range electrostatics and a 10 Å cutoff was set to treat real-space interactions. All covalent bonds involving hydrogen atoms were constrained with the SHAKE algorithm.[147] Each system was subject to a 100 ns MD simulation and the trajectory of simulated systems was saved every 100 ps.

3.0 RESULTS AND DISCUSSION

3.1 Innovation and Application of MCCS

Our lab has developed an innovative technique, MCCS, a method to quantify the energy contribution of residues involved in the interactions between compounds and protein(s) with high accuracy and high efficiency. Compared to molecular dynamics (MD) simulation-based energy decomposition, MCCS features the function to generate the binding recognition vector, the residue energy contribution, and vector similarity with high efficiency and high accuracy. The detailed protocol of MCCS could be found in our recent publication.[115] We also exploited MCCS in several applications or studies. The first study[148] was to analyze all the existing allosteric binding pockets in GPCRs regarding the interactions between important residues and AMs. Moreover, this study explored the detailed interaction within the allosteric binding pocket on CB1 and predicted the potential allosteric site(s) for CB2. The second study[149] was dedicated to repurposing and combining FDA-approved drugs with high efficiency, and also further designing new compounds for the treatment of COVID-19. The latest study[150] focused on the binding pockets in adenosine $A2_A$ receptor ($AA2_AR$), especially distinguishing the key residues binding with antagonists from that with agonists, analyzing various statuses of $AA2_ARs$, and investigating selectivity between $AA2_AR$ and adenosine $A1_A$ receptor ($AA1_AR$), which could facilitate the rational drug design for treatment involving $AA2_AR$. These studies served as a "proof-of-concept" of MCCS in that it can be applied by other researchers in the field for the design and discovery of functional ligands for a specific target.

3.2 Stabilization of Both GPCRs and Orthosteric Ligands by AMs

For GPCRs, there were four pairs of complexes of either X-ray crystals or cryo-EM structures, including M2 muscarinic acetylcholine receptor (M2 receptor), β2 adrenoceptor, and free fatty acid receptor 1 (FFA1/GPR40).

For the M2 receptor, PDB 4MQT is the complex of M2 muscarinic acetylcholine receptor, PAM-LY2119620, and agonist-iperoxo (**Figure 3a, magenta cartoon**), while PDB 4MQS is the complex of M2 muscarinic acetylcholine receptor with iperoxo (**Figure 3a, green cartoon**). There were no obvious conformational changes for both the orthosteric binding site and the whole structure of M2 when the two structures were aligned in PyMol (**Figure 3a**). Moreover, in the orthosteric binding pocket of the two structures, there was no residue with a significant change of the energy contribution (**Figure 3b**), indicating that the interactions between the orthosteric agonist and the receptor were stable after the binding of PAM. Recently, Kruse et al.[151] reported the binding affinity of iperoxo with/without LY2119620 using [^{3}H]-NMS competition binding assay. There wasn't a significant difference between the pKi values of iperoxo w/o the binding of LY2119620 (the pKi value of iperoxo with the binding of LY2119620 is 8.51 ± 0.04, and the Ki value for iperoxo without LY2119620 is 0.0073 μM, i.e., pKi value= 8.1367). Hence, our results were consistent with the experimental data and indicated that there was no significant conformational change in the orthosteric binding site of the M2 muscarinic acetylcholine receptor when a PAM binds at the allosteric binding site. On the other hand, there were only two residues, Trp422 and Phe181, that endured the conformational change in the allosteric binding pocket along with its energy contribution. When aligning the two structures, the conformation of the Trp422 side chain rotated from a horizontal pose to the vertical pose in the presence of LY2119620, which allowed the binding of LY2119620 to M2 to engage in an aromatic stacking interaction (**Figure**

3a). The side chain of Phe181 transformed from horizontal to vertical to the PAM, which accommodated the binding of LY2119620.

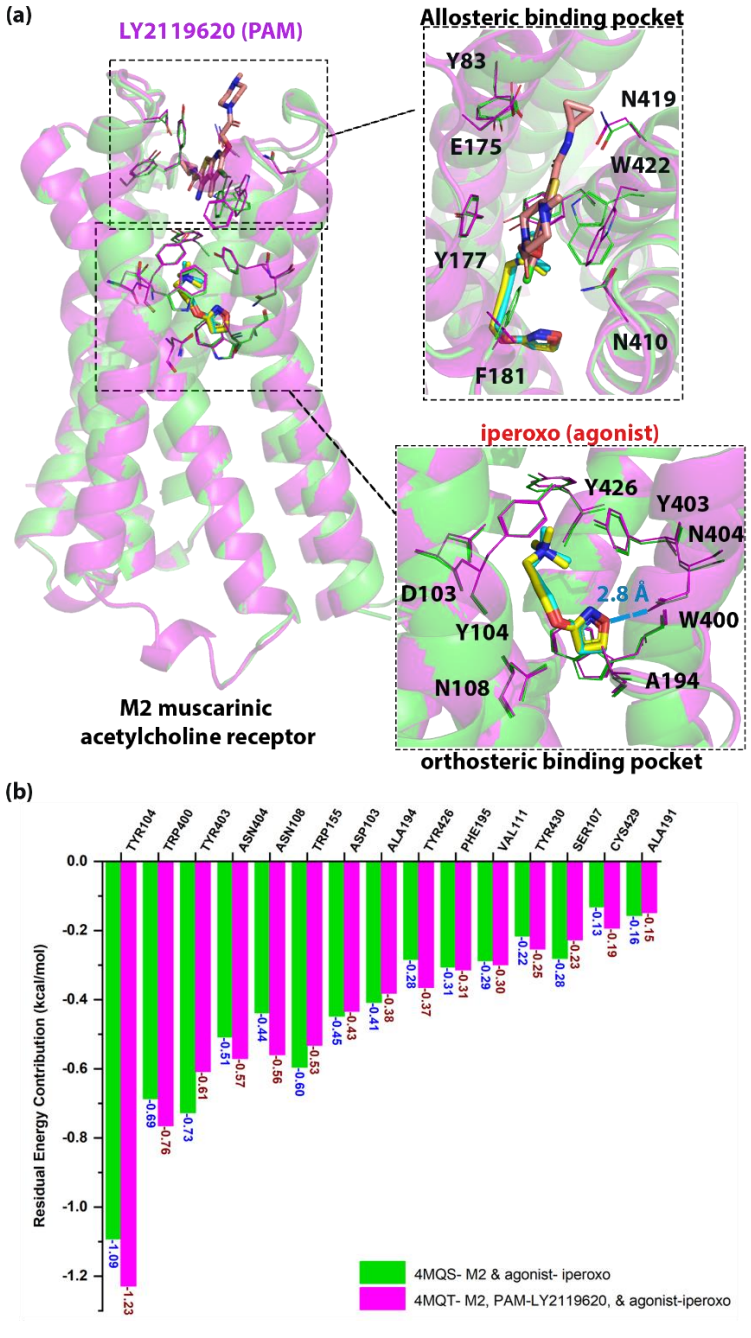

Figure 3. The comparison of the complex of M2-iperoxo(agonist) with/without the binding of the positive allosteric modulator (PAM)-LY2119620.

(a) The overlap of M2-iperoxo (green cartoon-blue stick) and M2-iperoxo-LY2119620 (magenta cartoon-yellow stick-salmon stick). The residues involved in the binding pockets are shown as thin element-colored lines. (b) The comparison of the binding residues involved in the orthosteric binding pocket between M2-iperoxo (PDB: 4MQS, green bars) and M2-iperoxo-LY2119620 (PDB: 4MQT, magenta bars).

There are two pairs for β2 adrenoceptors. The first pair is PDB 5X7D-2RH1, another pair consisted of PDB 6N48-4LDE. In the first pair, PDB 5X7D is the complex of β2 adrenoceptor, Compound 15 (Cmpd-15, NAM), and orthosteric antagonist carazolol, while PDB 2RH1 is the complex of β2 adrenoceptor binding with carazolol. In the orthosteric binding site (**Figure 4a**), most of the energy contributions of the residues were identical in the two structures, except for Asn293. The total free energy contribution of Asn293 reduced significantly when the NAM bound to the receptor. To be more specific, the steric force of Asn293 decreased greatly after the binding of Cmpd-15. Aligning the two structures showed that the position of Asn293 shifted for about 0.9 Å along with the slightly inward movement of TM6 caused by the NAM that stabilized the inactive conformation of the receptor (**Figure 4b**). It is worth noting that Asn293 is an important residue for interactions with both agonist and antagonist. A recent report by Wieland et al.[152] about the site-directed mutagenesis studies of Asn293 replaced by Leu supports that Asn293 is crucial for stereospecificity and intrinsic activity of agonists in their interactions with the receptor. Hanson et al.[153] reported a structure containing β2 adrenoceptor and timolol (PDB code: 3D4S), and their results showed that Asn293 played an important role in the interaction between the antagonist and β2 adrenoceptor. Our computational results agreed with the experimental data and further unveiled the detailed energetic change of residues. Finally, we also investigated the detailed interactions between NAM-Cmpd-15 and its surrounding residues. Most of the allosteric binding residues did not endure significant conformational changes, including Leu64, Asn69, Ala271, Thr274, Tyr326,

and Ser329. However, four residues, Arg63, Asp331, Lys267, and Phe332, rotated to either accommodate or interact with Cmpd-15.

In the second pair, PDB 6N48 is the complex of β2 adrenoceptor- orthosteric agonist BI167107- PAM compound-6FA, and PDB 4LDE is the complex of the β2 adrenoceptor-BI167107. The energy contribution of important residues in the orthosteric pocket did not endure significant change after the PAM bound to the receptor. The computed result is consistent with the alignment of the two structures that the residues in the orthosteric binding pocket only underwent slight movement when the PAM bound. In addition, in the allosteric binding site, Phe113, Tyr141, Leu144, and Lys149 rotated away from or approach to the pocket center to accommodate the PAM, while other residues only shifted along with the movement of helixes around the pocket.

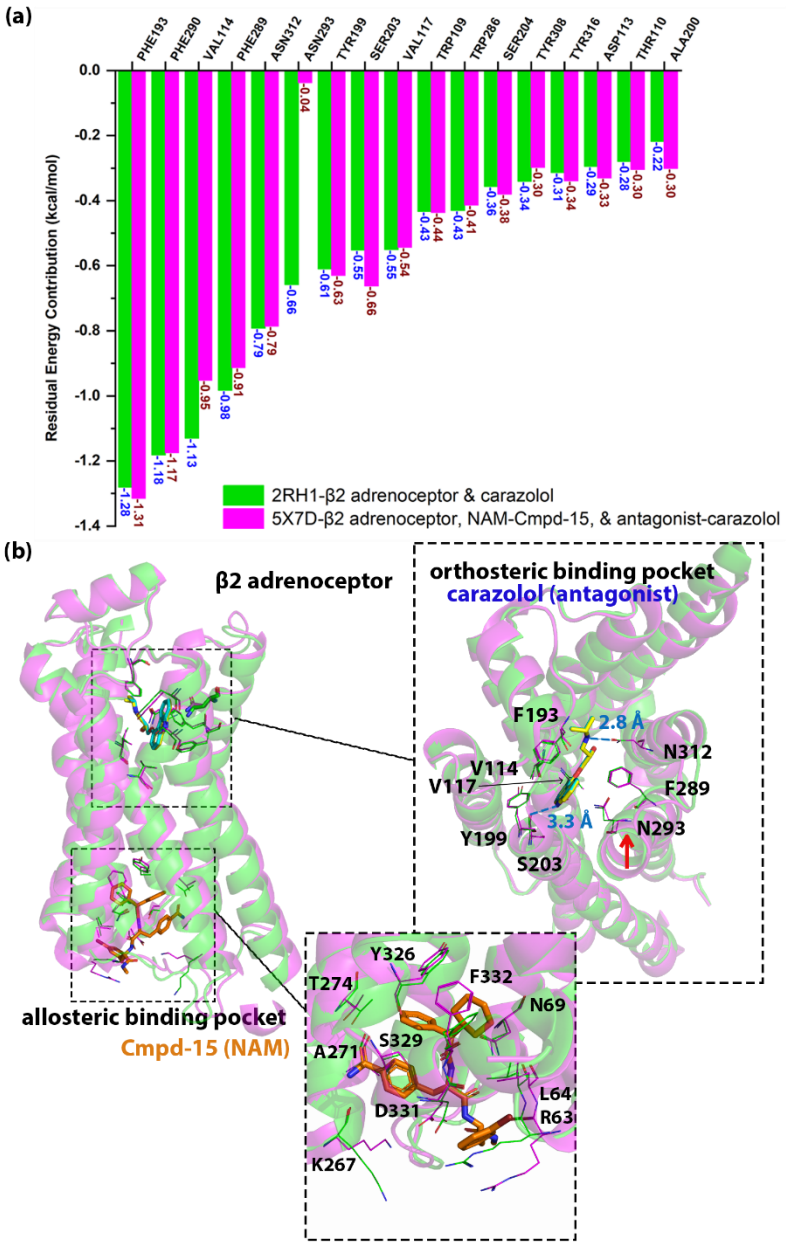

Figure 4. The comparison of the complex of β2-carazolol(antagonist) with/without the binding of the negative allosteric modulator (NAM)-Cmpd-15.

(a) The comparison of the binding residues involved in the orthosteric binding pocket between β2-carazolol (PDB: 2RH1, green bars) and β2-carazolol-Cmpd-15 (PDB: 5X7D, magenta bars). (b) The alignment of β2-carazolol (green cartoon-blue stick) and β2-carazolol-Cmpd-15 (magenta cartoon-yellow stick-orange stick). The residues involved in the binding pockets are shown as thin element-colored lines. The red arrow shows the inward movement of TM6.

For the FFA1 receptor, PDB 5TZY is the complex of FFA1, allosteric agonist AgoPAM AP8, and agonist MK-8666. PDB 5TZR is the complex of FFA1 and MK-8666. Two important residues including Trp174 and Leu186 underwent significant changes in their energy contributions when AgoPAM AP8 bound to the structure. The steric force of Trp174 decreased and the hydrophobic contribution disappeared in the 5TZY structure compared to that in the 5TZR complex, leading to the raise of the total free energy of Trp174 with the binding of PAM. As for Leu186, the steric contribution increased and the hydrophobic contribution emerged in the 5TZY structure compared to that in the 5TZR complex, resulting in the loss of the total free energy of Leu186 with the binding of AP8. The two aligned structures of 5TZY and 5TZR showed that the extracellular part of FFA1 in 5TZY, except for TM1/2, moved in a clockwise direction compared to that in 5TZR (from extracellular part to intracellular portion), and the intracellular part of FFA1 moved outward when the PAM bound to the receptor. However, most of the residues in the orthosteric binding pocket between 5TZY and 5TZR structures did not endure significant change, while Trp174 and Leu186 were the exceptions. The rotation of Trp174 changed with the movement of ECL2 and the position of Leu186 raised with the movement of TM5, which was congruous with our computing results. Besides, Sum et al.[154] published a study regarding the important residues for the orthosteric agonist recognition and the activation of FFA1, in which the site-directed mutagenesis experiment of L186F proves that Leu186 plays a crucial role in the receptor activation. In addition, most of the conformation of the important residues in the allosteric binding pocket shifted mildly along with the movement of helixes where they were located, while the side chain of Leu190 rotated to accommodate the binding of the PAM.

3.3 Stable Conformations and Interaction of the Enzymes-Orthosteric Ligand by AMs

There were 11 pairs of enzymes collected in the present study, and the receptors included 3-phosphoinositide-dependent protein kinase-1 (PDK1), dual specificity mitogen-activated protein kinase 1 (MEK1), Tyrosine-protein kinase ABL1, Glucokinase (GK), K-Ras GTPase, Acetylcholinesterase, Amine oxidase [flavin-containing] B (MAO-B), and mitochondrial glutamate dehydrogenase 1 (GDH 1). The results of 11 pairs of enzymes were similar in terms of the number of binding residues with significant conformational change (**Table 1** and **Table 2**).

For PDK1, PDB 3HRF is the complex of the kinase-PAM PS48-ATP, while PDB 3HRC is the complex of the kinase and ATP. After comparing the computing results of 3HRF and 3HRC, we found that two important residues, Ser92 and Ser94, were significantly different between the two structures. The binding of the PAM led to the rise of total free energy and repulsion contributions of both two residues and the increase of hydrogen bonding strength between Ser92 and the ligand. In addition, the total free energy of another two residues, Glu166 and Lys111, decreased mildly after the binding of PAM, but the constitution of the energy types changed significantly. The strength of the hydrogen bond raised in Glu166 and declined in Lys111. The steric force grew in Lys111 and fell off in Glu166. Aligning the two structures showed that PDK1s in both structures were nearly overlapped, except for the slight movement of β-sheets and the glycine-rich loop which were located at the upper part of the orthosteric binding pocket and moved inward in the complex with PAM. Moreover, the ribose and triphosphate group in the ATP in the 3HRF structure rotated slightly away from the glycine-rich loop when the PAM bound. Ser92 and Ser94 were on the glycine-rich loop, and the rotation of the oxygen side chain on Ser92 changed, which was consistent with our computing results. Previous studies have proved that the glycine-rich loop plays a key role in the activation of the protein, and Lys111 and Glu166 are well-known

key residues in ATP binding sites.[155-158] In addition, most of the important residues in the allosteric binding pocket did not undergo huge conformational change, except for Phe157 which rotated from vertical to horizontal pose when the PAM came to the pocket.

Another set of complexes for PDK1 showed similar results. PDB 4AW1 is the complex of the kinase-PAM PS210-ATP. PS210 is more potent than PS48 (IC50 value: PS210 with 39000 nM and PS48 with 97000 nM).[159] Compared to PDB 3HRC, the total free energies of Ser94, Lys111, Glu166, Glu209, and Asn210 in PDB 4AW1 were significantly different, and that of Ser92 increased moderately but the composition of energy types changed largely. Glu209 has been reported as an important residue for the binding of ATP via carbonyl oxygen.[158] The computing results were consistent with the observation of 3D structures. Aligning the two complexes, the conformation of β-sheets, αB-helix, αC-helix, and the glycine-rich loop moved inward when the PAM bound to the kinase. Notably, ATP in PDB 4AW1 rotated and moved downward along with the pushing down of the glycine-rich loop which converted PDK1 from an open-active state to a close-active conformation. Most of the residues in the orthosteric pocket did not endure significant conformational change, only the residues on the β-sheets and glycine-rich loop shifted along with the inward movement of the main structures. The reposition of those residues did not lead to significant change regarding the interaction with ATP since the position of ATP also shift along with the inward movement of β-sheets and glycine-rich loop. In addition, the important residues in the allosteric pocket only shifted along with β-sheets and α-helix, except for Phe157 which occurred the same conformational change as that in 3HRC.

For MEK1, there were two pairs of collected complexes. The first pair is PDB 3EQC and PDB 3EQD, the second one is PDB 3EQI and PDB 3EQH. PDB 3EQC is the complex of MEK1-ATP-γS-NAM Compound 1. PDB 3EQD is the complex of MEK1 and ATP-γS. PDB 3EQI is the

complex of MEK1 and ADP. PDB 3EQH is the complex of MEK1- ADP- NAM U0126. Based on the literature, MEK1 in these four complexes was in an inactive state,[155, 160-162] and the mechanisms of the two NAMs on the inactivation of MEK1 were different.

By comparing the binding characterization of the orthosteric binding site in PDB 3EQC with PDB 3EQD and in 3EQH with 3EQI, only one important residue-Lys97-underwent significantly change concerning the total free energy contribution (**Figure 6a**). In the first pair, when the NAM bound to the complex of MEK1- ATP-γS, the total free energy and the repulsion contribution of Lys97 sharply decreased. In the second pair, the total free energy, the repulsion, and the strength of the hydrogen bond of Lys97 declined significantly. According to literature, Lys97 plays an important role in the binding of ATP and inhibitors and is also a key residue in distinguishing the active and inactive state of MEK1.[155, 162-169] Aligning PDB 3EQC and PDB 3EQD, we found that the important residues in the orthosteric binding pocket in the two proteins are nearly overlapped (**Figure 6b**). The ribose and triphosphate group in the ATP-γS rotated slightly. Lys97 on the β sheets near the triphosphate group of ATP-γS was slightly rotating and shifting (about 0.3 Å with Cα as reference) along with the movement of β sheets. The result of aligning PDB 3EQH and PDB 3EQI is similar to that of the first pair. Similarly, we also found that the binding residues involved in the allosteric active site kept stable in the structure, as shown in **Figure 6b**; only a few residues, such as Leu215, Met219, and Val211, shifted along with the movement of the activation loop.

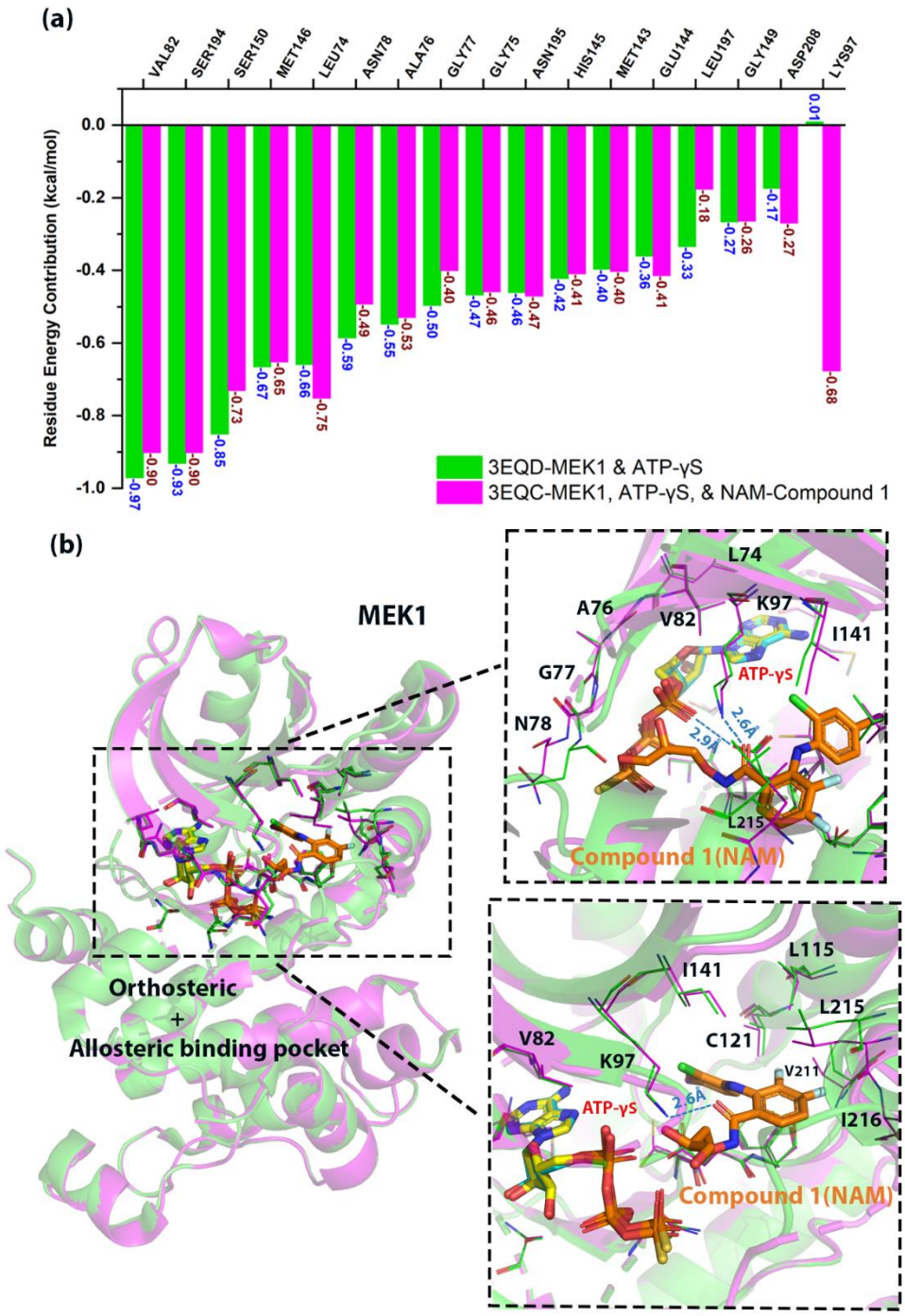

Figure 5. The comparison of the complex of MEK1-ATP-γS(agonist) with/without the binding of the negative allosteric modulator (NAM)-Compound-1.

(a) The comparison of the binding residues involved in the orthosteric binding pocket between MEK1-ATP-γS (PDB: 3EQD, green bars) and MEK1-ATP-γS-Compound-1 (PDB: 3EQC, magenta bars). (b) The

alignment MEK1-ATP-γS (green cartoon-blue stick) and MEK1-ATP-γS-Compound-1 (magenta cartoon-yellow stick-orange stick). The residues involved in the binding pockets are shown as thin element-colored lines.

For Tyrosine-protein kinase ABL1, there were also two pairs of complexes. The first pair was PDB 1OPK and PDB 2G2H. PDB 1OPK is the complex of the protein-inhibitor PD166326-NAM myristic acid. PDB 2G2H is the complex of the protein and PD166326. Comparing the computing results of PDB 1OPK with PDB 2G2H, only one important residue, Ala399, underwent a significant alteration of energy contribution after the binding of NAM. To be more specific, the total free energy of Ala399 declined, and the steric force of it increased. The second pair consisted of PDB 3PYY and PDB 2HYY, in which 3PYY is the complex of the protein-inhibitor imatinib-PAM DPH, and 2HYY is the complex of the protein-inhibitor imatinib. Comparing the computing results of PDB 3PYY with PDB 2HYY, we found that the total free energy of two important residues including His361 and Asp381 endured significant change. The total free energy of both residues declined and the steric force of them increased. The result of aligning the two structures showed that the protein structures around the orthosteric binding pocket and imatinib both had slight movement, and the rotation of carboxylate on Asp381 altered. In addition, the important residues in the allosteric binding pocket in the two pairs of complexes did not endure significant conformational change. Specifically, in the first pair of complexes, only a few residues shifted along with the outward movement of αE helix when the NAM inserted to the pocket, while in the second pair, some of the important residues only slightly shifted along with the slightly outward movement of the helixes around the binding site when the PAM inserted into the pocket.

For GK, PDB 3F9M is the complex of GK, substrate α-D-glucopyranose, and PAM-TAFMT, while PDB 3IDH is the complex of GK and α-D-glucopyranose. As shown in **Figure 5a**, the computed results of the orthosteric binding pocket in the two structures were almost identical,

and no residues underwent conformational change after the PAM bound (**Figure 5b)**. In addition, the residues involved in the allosteric pocket of PAM also did not endure significant conformation change, except for Tyr215 rotating toward the pocket center, and Thr65, as well as Pro66, moving along with the loop when the PAM bound to the pocket (**Figure 5b)**. Moreover, studies for site-directed mutagenesis of Tyr215 to Ala and a natural variant of Thr65 to Ile support that both residues play important roles in the interaction between GK and PAM. To be more specific, Y215A and T65I both raised the affinity of the glucose binding and the glucokinase activity which was measured by the catalytic efficiency.[170-172]

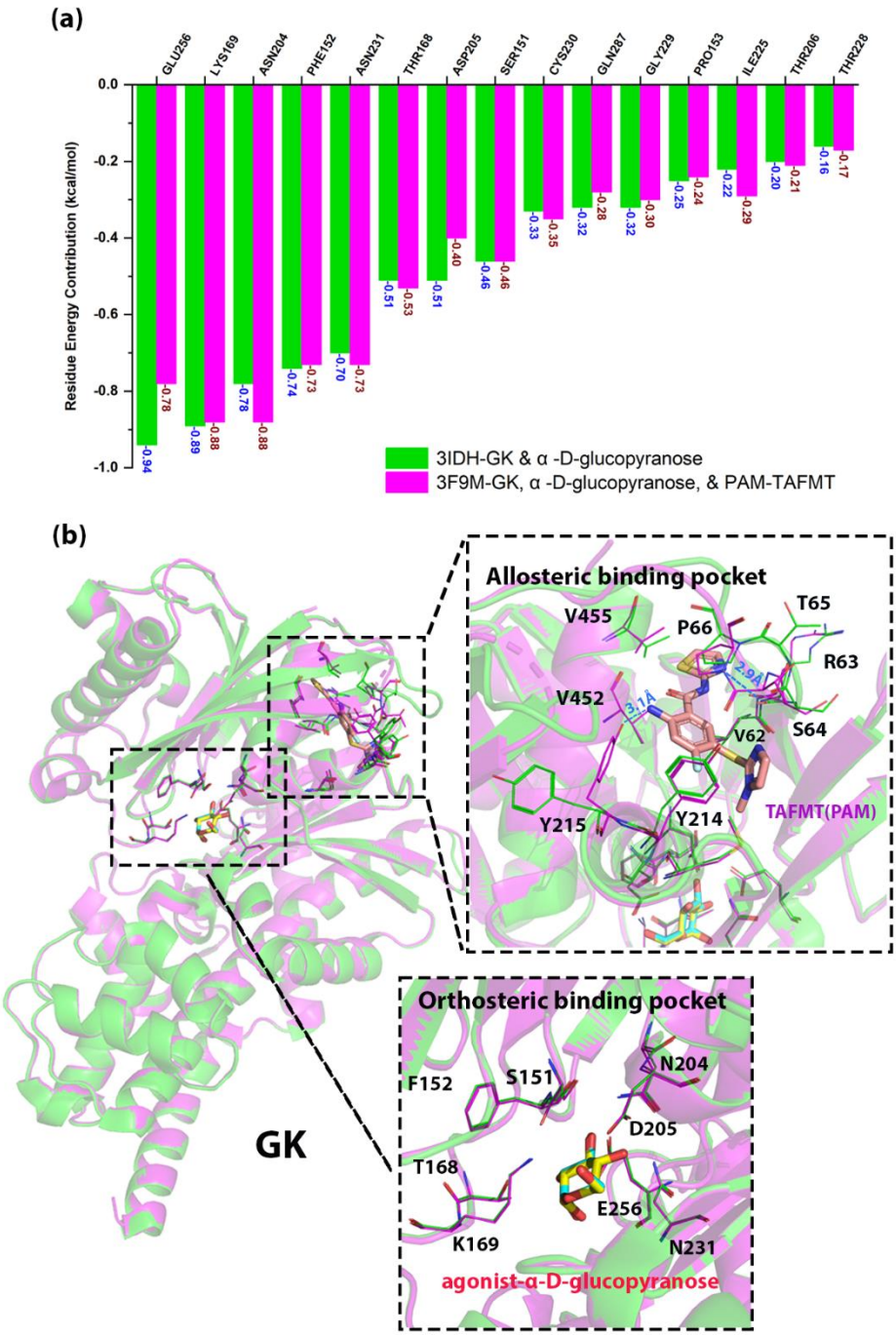

Figure 6. The comparison of the complex of GK-α-D-glucopyranose(agonist) with/without the binding of the positive allosteric modulator (PAM)-TAFMT.

(a) The comparison of the binding residues involved in the orthosteric binding pocket between GK-α-D-glucopyranose (PDB: 3IDH, green bars) and GK-α-D-glucopyranose(agonist)-TAFMT (PDB: 3F9M, magenta

bars). (b) The alignment of GK-α-D-glucopyranose (green cartoon-blue stick) and GK-α-D-glucopyranose(agonist)-TAFMT (magenta cartoon-yellow stick-salmon stick). The residues involved in the binding pockets are shown as thin element-colored lines.

For K-Ras GTPase, PDB 4M22 is the complex of the K-Ras G12C-inhibitor GDP- NAM acrylamide16, and PDB 4LDJ is the complex of the K-Ras G12C -GDP. K-Ras G12C is K-Ras GTPase with common oncogenic mutant G12C. Acrylamide 16 covalently binds to G12C and therefore does not have an impact on the normal protein. The total free energy contribution of residues in the orthosteric pocket of PDB 4M22 was similar to that of PDB 4LDJ, except for Asp30. When the NAM bound to the structure, the total free energy of Asp30 decreased and the steric force of it raised. Our result was consistent with the alignment of these two 3D structures that the rotation and the position of Asp30 altered along with the conformational change of the loop where Asp30 was located. Moreover, previous studies supported that the residues 29-35 were important nucleotide-binding region for GTP.[173, 174] Additionally, the allosteric binding pocket did not endure significant conformational change, except for the loop connecting α2 helix and β3 sheet where Gln61 and Arg68 were located. There were four important residues rotated after the NAM bound to the pocket. Specifically, Tyr96 rotated from the vertical pose into the pose that was parallel with the benzene ring of acrylamide16, Arg68 rotated towards the NAM, and Gln61, as well as Gln99, rotated away from the pocket.

For Acetylcholinesterase, PDB 5HF9 is the complex of the enzyme, inhibitor paraoxon which can covalently bond to the active site, and PAM HI-6 which is an oxime reactivator that can restore the enzyme activity. PDB 5HF5 is the complex of the enzyme and paraoxon. Comparing the computing results of two structures, only one residue, Phe295, underwent a significant change of the total free energy contribution when the PAM bound. To be more specific, the total free energy of Phe295 increased from -0.34 to 0.34 kcal/mol due to the sharply climbing of the

repulsion force. The result was consistent with the alignment of the two 3D structures. When the PAM bound to the protein, Phe295 approached to paraoxon along with the significant conformational change of the loop where Phe295 was located. In addition, in the allosteric binding site, the main structure and residues around the pocket did not endure significant change when the PAM bound to the pocket, except for Trp286 which rotated towards HI-6 and the indole on Trp286 became parallel to the pyridine on HI-6.

For MAO-B, PDB 2XFQ is the complex of MAO-B, inhibitor 2-(2-benzofuranyl)- 2-imidazoline (2-BFI), and NAM rasagiline which covalently connects with MAO-B. PDB 2XFN is the complex of MAO-B and 2-BFI. The total free energy of the important residues in the orthosteric binding pocket in the two structures were very similar, except for Leu167. The total free energy of Leu167 declined due to the raising of the steric force, which was consistent with the observation of the 3D structures. The results of aligning two structures showed that Leu167 rotated away from the pocket after the NAM was bound to the complex. In addition, the conformation around the allosteric pocket did not undergo significant change when the NAM bound to the protein.

For GDH 1, PDB 3ETG is the complex of GDH 1, glutamic acid, NADPH, GTP, and GW5074, among which GTP and NADPH are endogenous NAM, glutamic acid is the substrate, and GW5074 is NAM. PDB 6DHQ is the complex of GDH 1, glutamic acid, NADPH, and GTP. Comparing the computing results of the glutamic acid binding pocket of two complexes showed that most of the important residues had similar total free energy, except for four residues (Val378, Lys114, Lys90, and Met111), undergoing significant change when GW5074 bound. To be more specific, the total free energy of the four residues raised, the steric force of the four residues dropped, and the repulsion of Lys114, Lys90, and Met111 climbed greatly. The result of aligning

the two 3D structures showed that the four residues and glutamic acid rotated slightly. Furthermore, Li et al.[175] reported the binding affinity of glutamate with/without the GW5074. The Km value and Ki value of glutamate were all similar when the concentration of GW5074 raising from 0 μM to 8 μM. Additionally, most of the important residues in the allosteric binding site did not endure significant conformational change when the NAM bound, except for Lys143 which rotated away from the pocket.

3.4 Stability in Ion Channels and Transcription Factor

Five pairs of complexes belonged to ligand-gated ion channels in the present study, including a pair of AMPA receptor 2 (GluR-2), a pair of AMPA receptor 3 (GluR-3), two pairs of NMDA receptors (NMDARs), and a pair of Glutamate receptor, ionotropic, kainate 1 (GluK1). The results of five pairs of ion channels were similar, in which there were only zero to two binding residues in the orthosteric and allosteric sites undergoing significantly conformational change when an AM bound to the receptors (**Table 1** and **Table 2**).

AMPA receptors have two variants, flip and flop forms. Two complexes of GluR-2 are in the flip forms, while the structures of GluR-3 are both in flop form. For GluR-2, PDB 1LBC is the complex of GluR-2, substrate glutamate, and PAM cyclothiazide (CTZ). PDB 1FTJ is the complex of GluR-2 and glutamate. By comparing the important residues in glutamate binding pockets in the two structures, the energy contribution of them was similar, which was consistent with the alignment of the two 3D structures that the residues in the orthosteric binding site only shifted slightly along with the slight movement of the helixes and loops. Moreover, the important residues

in the allosteric binding site also did not endure significant change when the PAM came to the pocket.

For GluR-3, PDB 3M3F is the complex of GluR-3, flop-selective PAM 4-[2-(phenylsulfonylamino)ethylthio]-2,6- difluorophenoxyacetamide (PEPA), and substrate glutamate. PDB 3M3K is the complex of GluR-3 and glutamate. By comparing the two structures in terms of the glutamate binding pockets, the energy contribution of the important residues was similar, except for Arg509 and Glu731. Specifically, when the PAM bound to the receptor, the total free energy as well as the repulsion of the two residues declined, and the strength of hydrogen bonds in Arg509 reduced. Aligning the two 3D structures showed that both residues underwent mildly conformational change along with the mild movement of helixes around the binding site after the PAM existed. In addition, the important residues in the allosteric binding site also did not endure significant conformational change when the PAM was bound.

For NMDARs, we utilized two pairs of NMDARs in this study, including PDB 5H8H-5H8F and PDB 5H8N-5H8F. NMDARs are the complex of heterotetramers consisting of two NMDA 1 (GluN1) and typically two NMDR 2 (GluN2) subunits.[176] Activation of NMDARs requires glycine/D-serine, glutamate, and membrane depolarization.[177, 178] PDB 5H8F is the complex of GluN1-GluN2A-glycine- glutamate. PDB 5H8N is the complex of GluN1-GluN2A-glycine-glutamate- NAM compound 6. PDB 5H8H is the complex of GluN1-GluN2A-glycine-glutamate-PAM GNE3419. GNE3419 has been reported to have an impact on the interactions between glutamate and NMDARs.[179] By comparing the glutamate binding sites within each pair, the conformational change and energy contribution of the key binding residues in the orthosteric pockets were similar to each other (**Figure 7a and 7b**), indicating that the binding of PAM and NAM can stabilize the conformations of both ion channels and the orthosteric ligands.

Only a few residues underwent significant change in the allosteric binding pocket when an AM bound. Specifically, when the NAM bound to the pocket, Glu530 (GluN2A) rotated away from and Arg639 (GluN1) approached towards the NAM; while when the PAM bound to the pocket, Glu530 (GluN2A) and Tyr535 (GluN1) rotated away from the PAM to accommodate the binding of the compound.

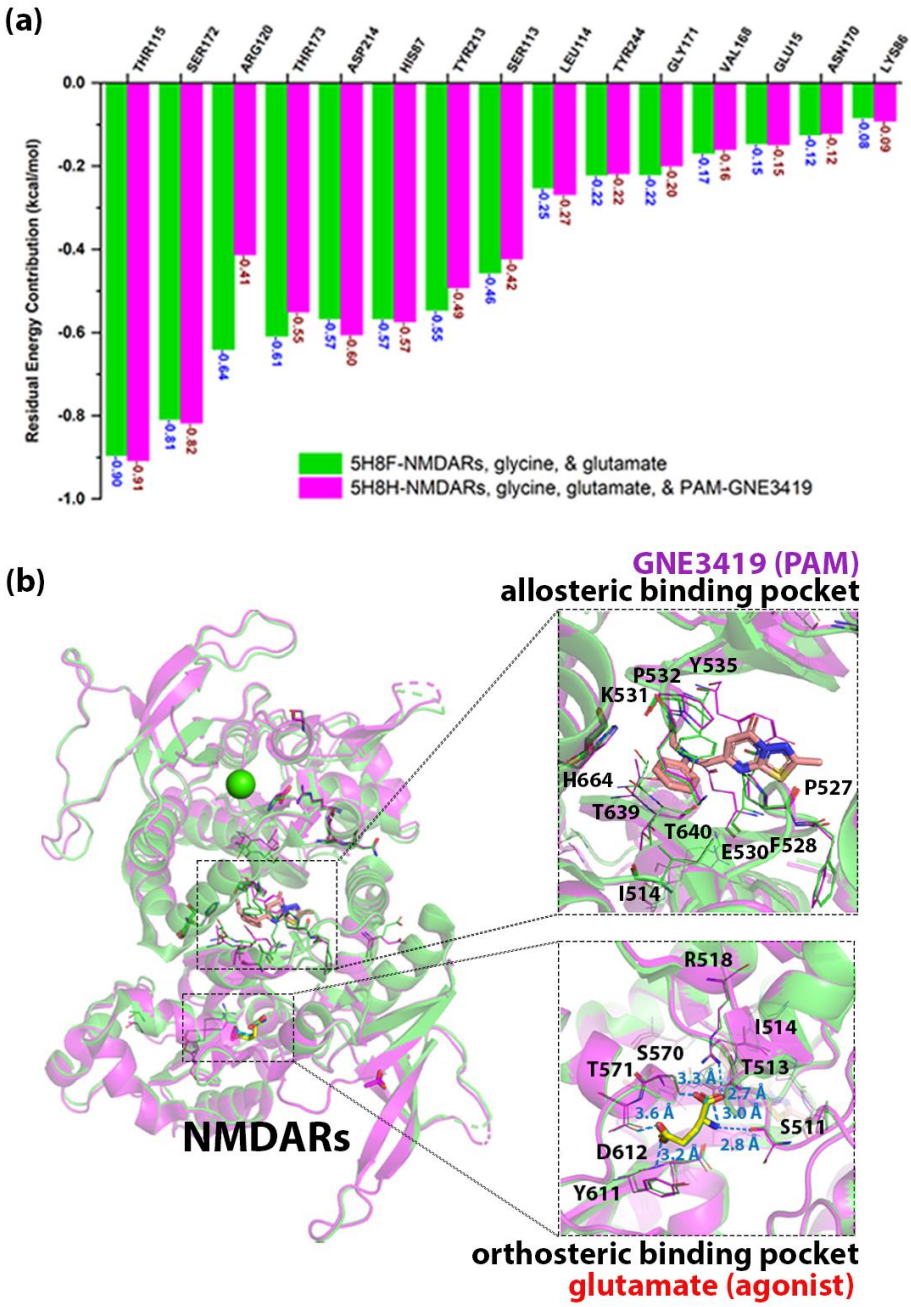

Figure 7. The comparison of the complex of NMDARs-glycine/glutamate with/without the binding of PAM-GNE3419.

(a) The energy contributions of the binding residues in the orthosteric binding pocket of NMDARs-glycine/glutamate (PDB:5H8F) are highlighted in green bars, while those of NMDARs-glycine/glutamate-GNE3419 (PAM, PDB:5H8H) are highlighted in magenta bars. (b) The alignment

of NMDARs-glycine/glutamate (green cartoon-blue stick) and NMDARs-glycine/glutamate-(PAM) GNE3419 (magenta cartoon-yellow stick-salmon stick). The residues involved in the binding pockets are shown as thin element-colored lines.

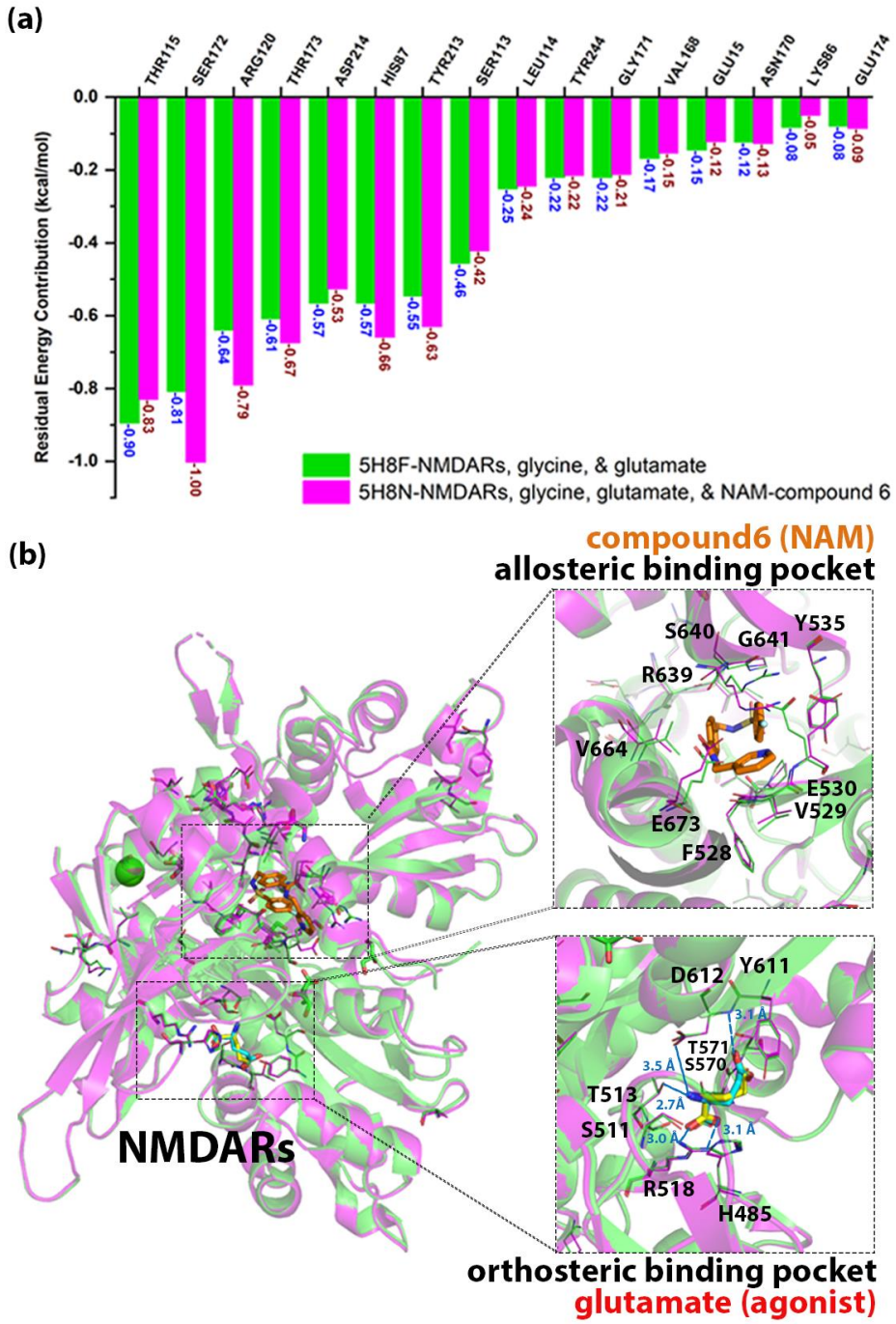

Figure 8. The comparison of the complex of NMDARs-glycine/glutamate with/without the binding of NAM-compound 6.

(a) The energy contributions of the binding residues in the orthosteric binding pocket of NMDARs-glycine/glutamate (PDB:5H8F) are highlighted in green bars, while those of NMDARs-glycine/glutamate-compounds 6 (NAM, PDB:5H8N) are highlighted in magenta bars. (b) The alignment of NMDARs-glycine/glutamate (green cartoon-blue stick) and NMDARs-glycine/glutamate- (NAM) compound 6 (magenta cartoon-yellow stick-orange stick). The residues involved in the binding pockets are shown as thin element-colored lines.

For GluK1, PDB 5MFQ is the complex of GluK1-PAM BPAM-344- kainite, and PDB 4E0X is a complex of GluK1-kainate. By comparing the energy contribution of important residues in the orthosteric binding site, the energy binding pattern was similar in the two structures, which was consistent with the aligning result of the two complexes. Moreover, the important residues in the allosteric site also did not undergo significant conformational change when the PAM was bound.

Androgen receptor (AR) is the only transcription factor collected in this study. PDB 2YHD is the complex of AR, agonist testosterone (TES), NAM 4-(2,3-dihydro-1H-perimidin-2-yl) benzene-1,2-diol, while PDB 2AM9 is the complex of AR and TES. By comparing the TES binding pocket in the two complexes, we found that the total free energy contribution of each important residue was similar (**Figure 9a**), yet the energy composition of Arg752 changed (**Figure 10**). When the NAM bound, the repulsion force dropped and the strength of hydrogen bonds in Arg752 declined. The result was consistent with the observation of aligning the two 3D structures as shown in **Figure 9b**. The binding of NAM only caused slight conformational change except for the outward movement of helix-10 to approach helix 9. The side chain of Arg752 twisted about 20 degrees when the NAM bound to AR. In addition, the allosteric binding residues did not endure huge conformational changes except for Met734 rotating away from the pocket center when the NAM came to the pocket.

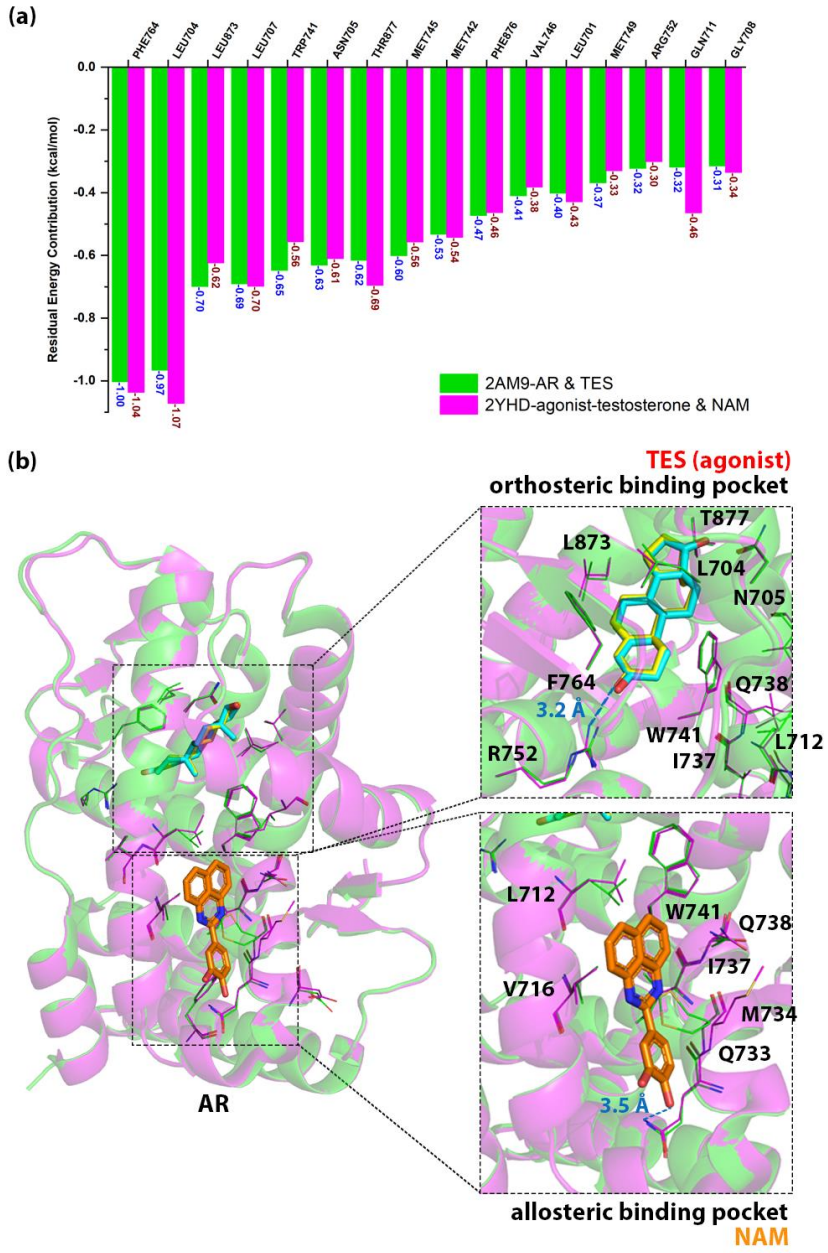

Figure 9. The comparison of the complex of AR-testosterone (TES) with/without the binding of negative allosteric modulator (NAM)- 4-(2,3-dihydro-1H-perimidin-2-yl) benzene-1,2-diol.

(a) The energy contributions of the binding residues of AR-testosterone (TES) (PDB:2AM9) are highlighted in green bars, while the energy contributions of the binding residues of AR-testosterone (TES)-NAM (PDB:2YHD) are highlighted in magenta bars. (b) The alignment AR-testosterone (TES) (green cartoon-blue stick) and AR-testosterone (TES)-NAM (magenta cartoon-yellow stick-orange stick). The residues involved in the binding pockets are shown as thin element-colored lines.

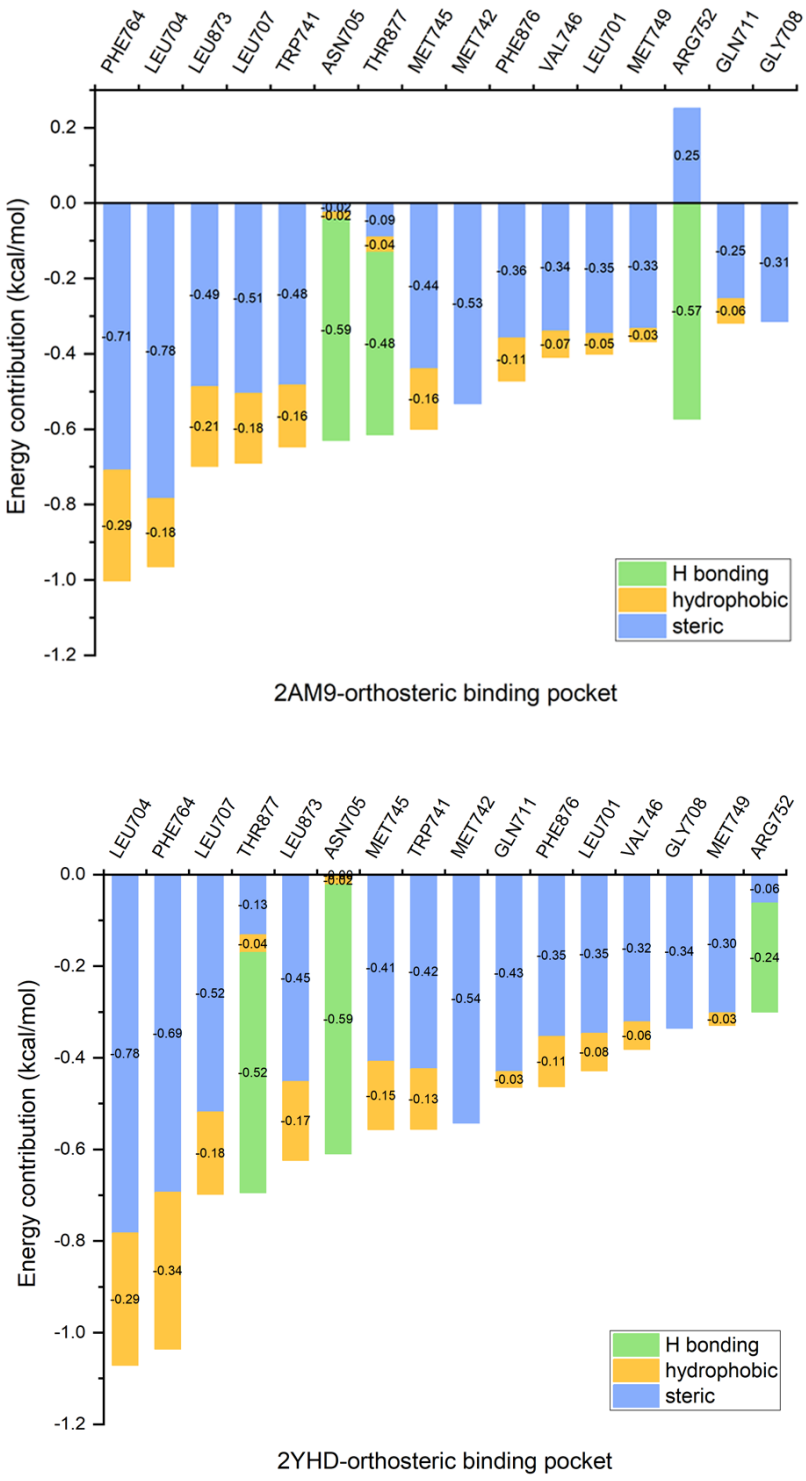

Figure 10. The detailed energy contributions of important binding residues in the orthosteric pocket of AR. Blue bars are steric force, yellow bars are hydrophobic interaction, and green bars represent hydrogen bonding strength. PDB 2AM9 is the complex of AR-TES. PDB 2YHD is the complex of AR-TES-NAM.

3.5 Comparison of Orthosteric and Allosteric Binding Sites Between the 21 Pairs X-Ray Crystal or Cryo-EM Complexes

According to the pharmacological features of the ligands in complexes, 21 pairs could be divided into 2 groups that were (1) agonist with PAM and antagonist with NAM (**Table 1**), and (2) agonist with NAM and antagonist with PAM (**Table 2**). In the first group with sixteen pairs of structures, AMs have little impact on the conformation of the orthosteric binding pocket. To be more specific, most of them only have one or two binding residues undergoing significant conformational change after an AM bound to the receptors. On the other hand, in the second group with five pairs of complexes, we also found the binding of AM did not lead to a significant change in the interaction between orthosteric compounds and the protein. Specifically, four of them with no more than two important residues and one pair with four residues underwent significant change.

Moreover, aligning the complexes within each pair showed that the structure around the allosteric binding sites did not endure significant conformational change when an AM was bound to the pocket: most of the important residues only shifted mildly when the α-helixes or β-sheets that were around the allosteric pocket moved slightly. However, in some of the allosteric binding sites, a few residues which possessed a large side chain may have either rotated away from or approached the allosteric binding pocket to accommodate the binding of AMs. Based on the findings above, we observed that the binding of AM had little impact on the conformation of both the orthosteric- and allosteric-binding pockets.

To further validate our results, we calculated the RMSD value within each pair of complexes to compare the whole protein structures, orthosteric binding sites, and allosteric binding pockets. As shown in **Table 2** and **Table 3,** all the RMSD values are smaller than 1 Å, indicating

that the conformation of the protein structures and their pockets did not undergo significantly conformational change when an AM bound to a specific protein.

In addition, most of the rotated residues in allosteric pockets play important roles in the binding of AM. Take the M2 receptor as an example, with in-silico site-mutagenesis of W422A, the normalized total binding free energy between the residues and LY2119620 dropped from -7.484 kcal/mol to -6.161 kcal/mol. However, the residues in the AM pocket which did not undergo significant conformational change did not mean they are not important for the AM binding. The calculation with MCCS can identify the important residues in AM pockets. Take Y177 in M2 receptor as another example for residues without undergoing significant rotation during the binding of AM, the in-silico results showed that Y177 in PDB 4MQT structure contributed binding free energy of -1.555 kcal/mol for the interaction with LY2119620, while Y177A mutant contributed free energy with -0.637 kcal/mol and lead to the reduction of total binding free energy from -7.484 kcal/mol to -6.774 kcal/mol. Our predictions were consistent with recent studies: e.g., Valant C et. al[180] reported the binding affinity of NAM gallamine for Y177A mutant drop with an 18.621-fold change of Ki value, and Gregory KJ et. al[181] published the Ki value for the binding of PAM 77-LH-28-1 for Y177A mutant increase with a 3.165 foldchange.

Table 2. Sixteen pairs of complexes consisted of either agonist with PAM or antagonist with NAM.

Receptor	PDB	Compounds in PDB	Residues with a significant change in the orthosteric pocket	Residues rotate in the allosteric pocket when AM bound	RMSD of the whole protein (Å)	RMSD of the orthosteric binding sites (Å)	RMSD of the allosteric binding pockets (Å)
M2 muscarinic acetylcholine receptor	4MQT	PAM: LY2119620, agonist: iperoxo	NA	Trp422, Phe181	0.195	0.158	0.249
	4MQS	agonist: iperoxo					
β2 adrenoceptor	5X7D	NAM: Cmpd-15, antagonist: carazolol	Asn293	Arg63, Asp331, Lys267, Phe332	0.355	0.291	0.312
	2RH1	antagonist: carazolol					
	6N48	PAM: compound-6FA, agonist: BI-167107	NA	PHE133, TYR141, LEU144, LYS149	0.303	0.224	0.373
	4LDE	agonist: BI-167107					
FFA1 (GPR40)	5TZY	PAM: AP8, agonist: MK-8666	Trp174, Leu186	LEU190	0.990	0.656	0.631
	5TZR	agonist: MK-8666					
PDK1	3HRC	ATP	Ser92, Ser94	Phe157	0.183	0.163	0.271
	3HRF	PAM:PS48, ATP					
	3HRC	ATP	Ser94, Lys111, Glu166, Glu209, Asn210	Phe157	0.297	0.536	0.626
	4AW1	PAM: PS210, ATP					
MEK1 (nonphosphorylated MEK1)	3EQC	NAM: Compound 1, ATP-γS	Lys97	NA	0.210	0.184	0.286
	3EQD	ATP-γS					
	3EQH	NAM: U0126, ADP	Lys97	NA	0.203	0.187	0.284
	3EQI	ADP					
Tyrosine-protein kinase ABL1	1OPK	NAM: myristic acid, inhibitor: PD166326	Ala399	NA	0.452	0.000	0.363
	2G2H	Inhibitor: PD166326					
GK	3F9M	PAM: TAFMT, agonist: α-D-glucopyranose	NA	Tyr215, Thr65, Pro66	0.291	0.132	0.286
	3IDH	agonist: α-D-glucopyranose					

K-ras-gtpase	4M22	NAM: acrylamide 16, GDP	Asp30	Tyr96, Arg68, Gln61, Gln99	0.332	0.218	0.279
	4LDJ	GDP					
Amine oxidase	2XFQ	NAM: rasagiline, 2-BFI, FAD	Leu167	NA	0.150	0.183	0.152
	2XFN	2-BFI, FAD					
AMPA GluR2	1LBC	PAM: cyclothiazide (CTZ), glutamate	NA	NA	0.423	0.233	0.348
	1FTJ	glutamate					
AMPA GluR3	3M3F	PAM: PEPA, glutamate	Arg515 Glu612	NA	0.522	0.343	0.369
	3M3K	glutamate					
NMDAR	5H8H	PAM: GNE3419, glutamate, glycine	NA	Glu530 (GluN2A), Tyr535 (GluN1)	0.637	0.148	0.337
	5H8F	glutamate, glycine					
GluK1	5mfq	PAM: BPAM-344, Kainate	NA	NA	0.443	0.233	0.221
	4e0x	Kainate					

Table 3. Five pairs of complexes comprised of either agonist with NAM or antagonist with PAM.

Receptor	PDB	Compounds in PDB	Residues with a significant change in the orthosteric pocket	Residues rotate in the allosteric pocket when AM bound	RMSD values for protein structures	RMSD values for orthosteric binding sites	RMSD values for allosteric binding pockets
Tyrosine-protein kinase ABL1	3PYY	PAM: DPH, inhibitor: imatinib	His361 Asp381	NA	0.340	0.287	0.363
	2HYY	inhibitor: imatinib					
Acetylcholinesterase	5HF9	PAM: HI-6, inhibitor: DEP	Phe295	Trp286	0.277	0.132	0.188
	5HF5	inhibitor: DEP					
GDH 1	3ETG	NAM: GW5074, glutamic acid, GTP, NADPH	Val378 Lys114 Lys90 Met111	Lys143	0.291	0.214	0.188
	6DHQ	glutamic acid, GTP, NADPH					
NMDAR	5H8N	NAM: compound 6, glutamate, glycine	NA	Glu530 (GluN2A), Arg639 (GluN1)	0.260	0.163	0.338
	5H8F	glutamate, glycine					
AR	2YHD	NAM: 4-(2,3-dihydro-1H-perimidin-2-yl) benzene-1,2-diol, TES	NA	Met734	0.253	0.207	0.232
	2AM9	TES					

3.6 Molecular Dynamics Simulation Studies

Molecular dynamic simulation studies were conducted to investigate the stability and dynamics of the PDB structures collected in this study. Here we selected two pairs of complexes: one is PDB 4MQS-4MQT consisting of M2 receptor, agonist iperoxo, and PAM LY2119620; another is PDB 2RH1-5X7D comprised of β2 adrenoceptor, antagonist carazolol, and NAM Cmpd-15.

As shown in **Figure 11**, the complex of PDB 4MQS and PDB 4MQT were stable during the simulation with the RMSD values of the receptor, the agonist, and the PAM in each complex were all under 5 Å. Specifically, the M2 receptor without the PAM was stable in the active state with the RMSD value around 2 Å, while the M2 receptor with the binding of PAM was more stable with the RMSD value around 1.5 Å, indicating that the binding of PAM stabilized the M2 receptor in an active state. **Figures 12a** and **12b** show the overlay of the first and the last frames of the simulation, portraying the dynamic conformational variation of the receptors and ligands during the simulation time. To evaluate that the binding of PAM does not lead to a significant conformational change of the orthosteric binding pocket, we aligned the last frames of the simulation of PDB 4MQS and 4MQT (**Figure 12c**). The residues in the orthosteric site moved along with the helixes where they were located but did not undergo a significant conformational change. **Figure 12c** also shows the G protein binding site of the M2 receptor with the alignment of the last frames of the simulation for the receptor w/o PAM as well as the cryo-EM structure of M2 receptor complexed with the same agonist, PAM and plus, the G protein subunits (PDB:6OIK). The intracellular portion of TMs 3,5,6,7 and helix 8 in both complex w/o PAM moved outward during the simulation, leaving a larger space for the insertion of the G protein α subunit. Specifically, the intracellular part of TMs 5,6,7 and helix 8 in the complex with PAM rotated and twisted much away from the center of the G protein binding site than that of the complex without PAM during the simulation course. PDB 6OIK showed that after coupling with G protein, TMs 5,6,7, and helix 8 moved inward to accommodate the α5 helix of G protein. The alignment of the three structures indicates that the binding of PAM allows the M2 receptor to couple with G protein more easily with a larger space at the G protein binding pocket, while the binding of G protein may lead to the reduction of the binding site volume for tighter interaction.

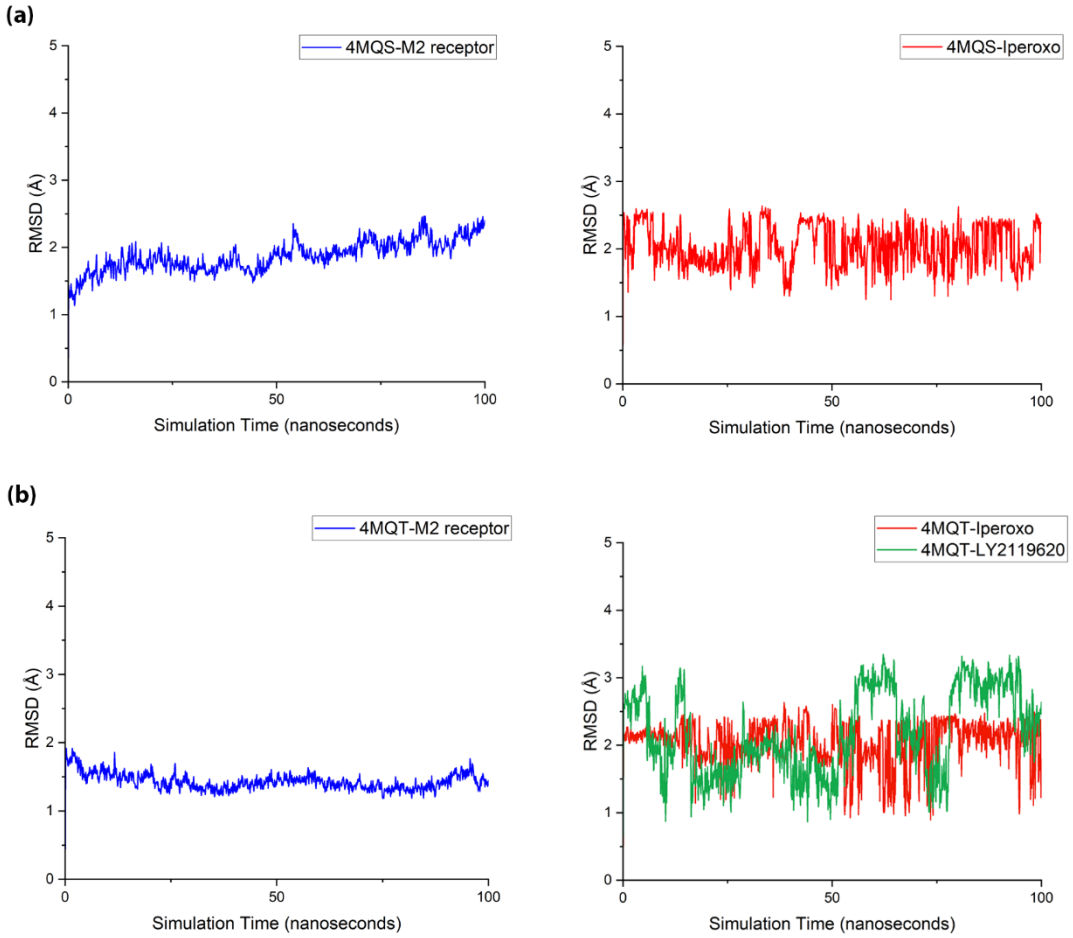

Figure 11. RMSD of PDB 4MQT-4MQS structures during MD simulation course.

The time course of RMSD of mainchain atoms of the M2 receptor (black), heavy atoms of agonist-iperoxo (red), and PAM LY2119620 (blue). (a) PDB 4MQS, (b) PDB 4MQT.

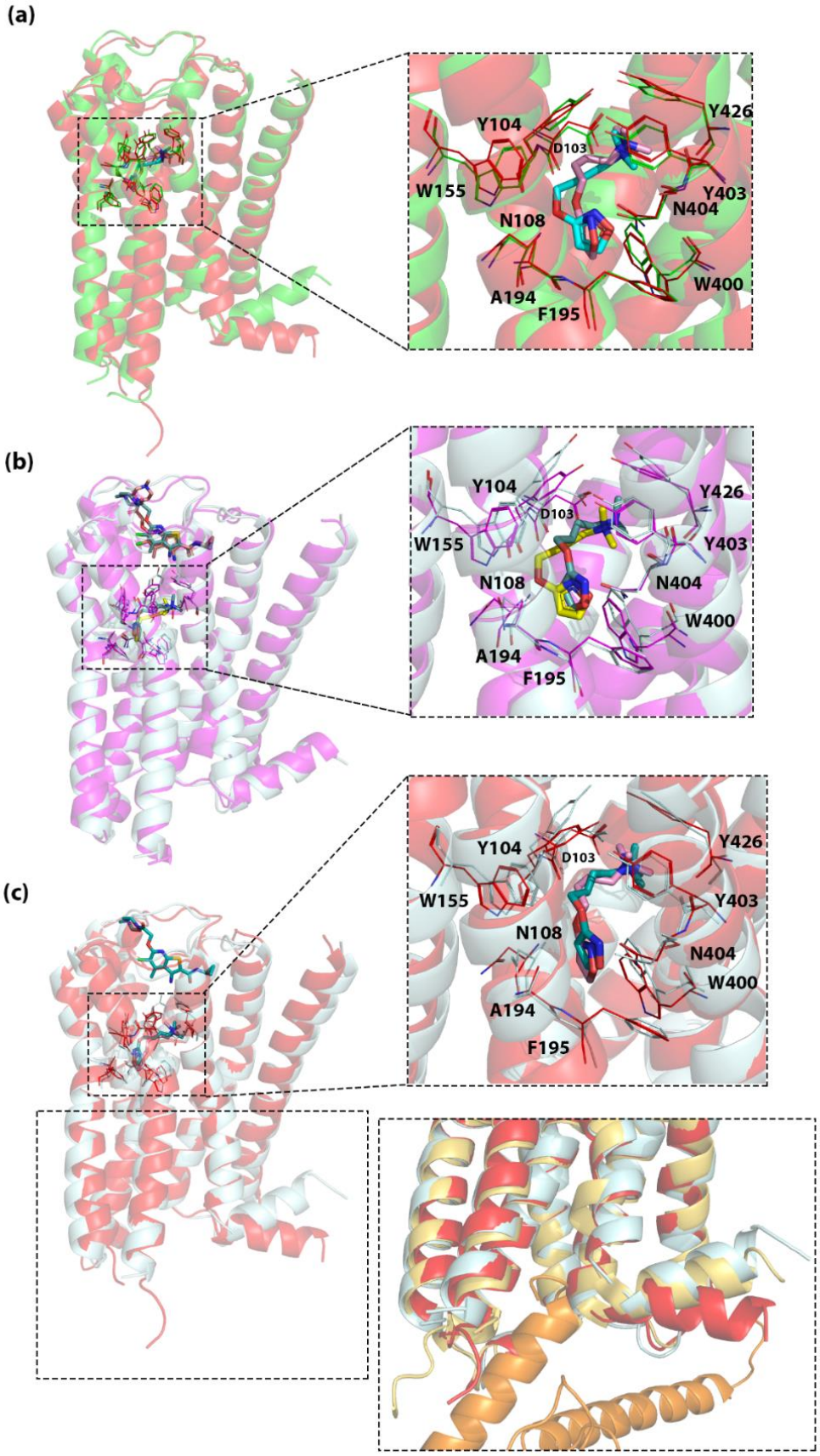
(a)
Y104
D103
Y426
W155
Y403
N404
N108
W400
A194
F195
(b)
Y104
D103
Y426
W155
Y403
N108
N404
W400
A194
F195
(c)
Y104
D103
Y426
W155
Y403
N108
N404
W400
A194
F195

Figure 12. MD simulation studies of PDB 4MQT-4MQS structures.

(a), (b) The overlay of the first and last frames of each of the two MD simulations. (a) the first frame of the receptor (green cartoon) and the agonist (cyan stick) and the last frame of the receptor (red cartoon) and the agonist (pink stick) in PDB 4MQS. (b) the first frame of the receptor (magenta cartoon), the agonist (yellow stick) and the PAM (salmon stick), and the last frame of the receptor (pale-cyan cartoon), the agonist (teal stick) and the PAM (teal stick) in PDB 4MQT. (c) the overlay of the last frames of the two MD simulations and the intracellular part of the overlay of the last frames of the two MD simulations as well as the PDB 6OIK structure. The color of the receptor and the ligands are the same as those in (a) and (b). The receptor in PDB 6OIK is shown as yellow-orange cartoon, and the Gα protein is shown as orange cartoon. Important residues in the orthosteric pocket are shown as lines.

For PDB 2RH1-5X7D, the NAM stabilized the receptor at the inactive state, which was delineated by **Figure 13**. During the simulation, the receptor in PDB 2RH1 kept stable with RMSD value oscillated around 2 to 3 Å, while the protein in PDB 5X7D was more stable than that in PDB 2RH1, with RMSD value fluctuating around 1.5 to 2.5 Å in the first 40 nanoseconds and around 1.5 to 2 Å for the last 60 nanoseconds. The alignment of the first and the last frames of the simulation of the two complexes in **Figures 14a** and **14b** delineate the geometrical variation of the β2 adrenoceptor, antagonist, and NAM during the simulation course. **Figure 14c** shows the alignment of the last frame of the simulation of the receptor w/o NAM, which demonstrated that the binding of NAM did not result in a significant conformational change in the orthosteric binding site.

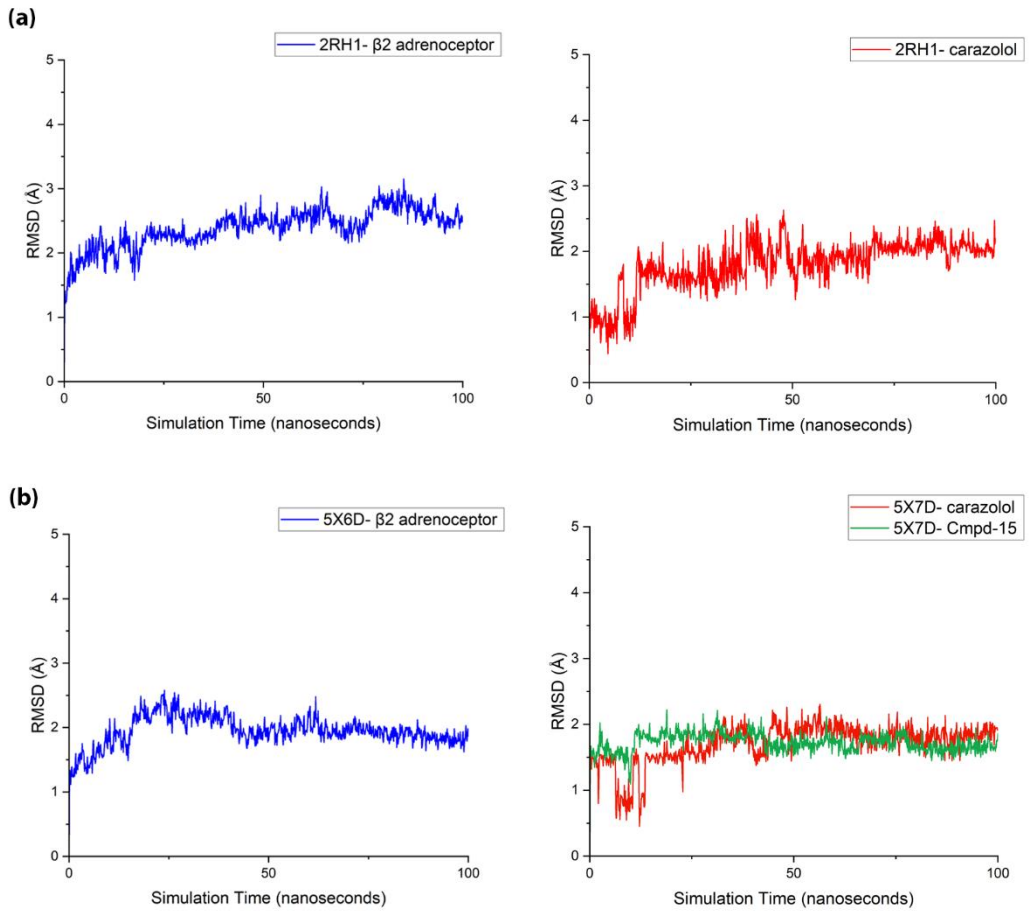

Figure 13. RMSD of PDB 5X7D-2RH1 structures during MD simulation course.

The time course of RMSD of mainchain atoms of the β2 adrenoceptor (blue), heavy atoms of antagonist carazolol (red), and NAM Cmpd-15 (green). (a) PDB 2RH1, (b) PDB 5X7D.

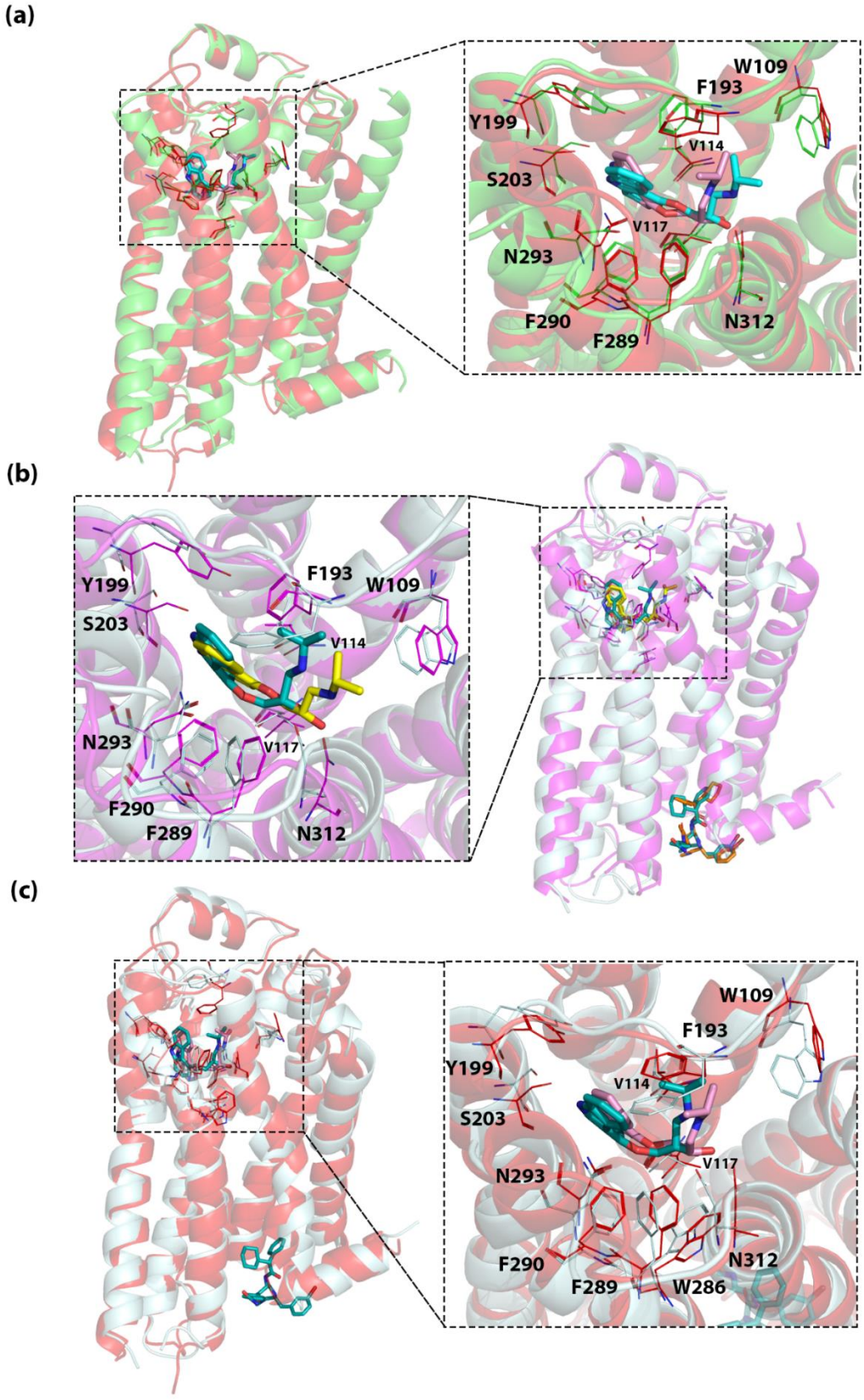
(a)
W109
F193
Y199
V114
S203
V117
N293
F290
F289
N312
(b)
Y199
F193
W109
S203
V114
N293
V117
F290
F289
N312
(c)
W109
F193
Y199
V114
S203
V117
N293
F290
F289
W286
N312

Figure 14. MD simulation studies of PDB 5X7D-2RH1 structures.

(a), (b) The overlay of the first and last frames of each of the two MD simulations. (a) the first frame of the receptor (green cartoon) and the agonist (cyan stick) and the last frame of the receptor (red cartoon) and the agonist (pink stick) in PDB 2RH1. (b) the first frame of the receptor (magenta cartoon the antagonist (yellow stick) and the NAM (salmon stick), and the last frame of the receptor (pale-cyan cartoon), the antagonist (teal stick) and the NAM (teal stick) in PDB 5X7D. (c) the overlay of the last frames of the two MD simulations. The color of the receptor and the ligands are the same as those in (a) and (b). Important residues in the orthosteric pocket are shown as lines.

4.0 CONCLUSION

When an AM bound to a target protein complexed with orthosteric ligand, it stabilizes the complex of protein-ligand into an active, inactive, or intermediate state, and may lead to a mild conformational change of the whole protein structure. However, there was no evidence regarding the influences of the binding of AMs on the orthosteric binding pocket and the allosteric ones. In the present study, we exploited an innovative technique, MCCS, which was developed by our lab and can characterize the interactions between compounds and protein to analyze 21 pairs of 3D crystal or cryo-EM complexes of protein-ligand-AM, including 4 pairs of GPCRs, 5 pairs of ion channels, 11 pairs of enzymes, and 1 pair of transcription factors. The results demonstrated that the binding of AM has few impacts on either conformation or energy contribution of the residues involved in the interactions between protein and the orthosteric ligand. Moreover, the binding of AMs did not cause a significant conformational change of allosteric binding pocket(s), and only a few residues with a large side chain may rotate away or approach towards the AMs. MD simulation studies supported that the structure of the protein and ligands are stable under dynamic circumstances.

Based on the results of this study, if the allosteric binding pocket(s) was predicted accurately, we can confidently conduct virtual screening as well as lead compound-based optimization for the AMs. Especially, our lab is dedicated to designing AMs for CB2 receptor which has neither X-ray crystal nor cryo-EM structures of CB2-orthosteric ligand-AM complex. We can first predict potential allosteric binding sites, and then conduct virtual screening and lead optimization for the development of CB2 AM drugs. Similarly, many target proteins do not have X-ray crystal and cryo-EM structures with AM. We can design the potential allosteric modulator

hits for them by virtual screening and lead optimization using the structure of protein-orthosteric ligand complexes. In summary, our study can facilitate the rational design and development of allosteric drug candidates.

Nonetheless, there are some limitations in this study. First, X-ray crystal and cryo-EM structures for many receptors are limited or unavailable, which restrains the diversity and the volume of the dataset. In addition, MCCS, the method used in the present work still has some limitations. For example, only the static structures/conformations that captured by X-ray crystal and cryo-EM methods, have been analyzed by MCCS. The MD simulation studies are to supplement the results under dynamic circumstances. Moreover, we will keep optimizing the MCCS to minimize the protein in the preparation steps and be able to conduct flexible docking.

Bibliography

1. Chen, I., *Allostery through DNA.* Nat Struct Mol Biol, 2013. **20**(4): p. 410.
2. He, X., et al., *Characteristics of Allosteric Proteins, Sites, and Modulators*, in *Protein Allostery in Drug Discovery*, J. Zhang and R. Nussinov, Editors. 2019, Springer Singapore: Singapore. p. 107-139.
3. Greener, J.G. and M.J. Sternberg, *Structure-based prediction of protein allostery.* Curr Opin Struct Biol, 2018. **50**: p. 1-8.
4. Dokholyan, N.V., *Controlling Allosteric Networks in Proteins.* Chem Rev, 2016. **116**(11): p. 6463-87.
5. Hertig, S., N.R. Latorraca, and R.O. Dror, *Revealing Atomic-Level Mechanisms of Protein Allostery with Molecular Dynamics Simulations.* PLoS Comput Biol, 2016. **12**(6): p. e1004746.
6. Zhang, J., et al., *Conformational transition pathway in the allosteric process of human glucokinase.* Proc Natl Acad Sci U S A, 2006. **103**(36): p. 13368-73.
7. Cong, X., et al., *Allosteric modulation of protein-protein interactions by individual lipid binding events.* Nat Commun, 2017. **8**(1): p. 2203.
8. Das, D. and B.A. Krantz, *Peptide- and proton-driven allosteric clamps catalyze anthrax toxin translocation across membranes.* Proc Natl Acad Sci U S A, 2016. **113**(34): p. 9611-6.
9. Kim, S., et al., *Probing Allostery Through DNA.* Science, 2013. **339**(6121): p. 816-819.
10. Lu, S. and J. Zhang, *Small Molecule Allosteric Modulators of G-Protein-Coupled Receptors: Drug-Target Interactions.* J Med Chem, 2019. **62**(1): p. 24-45.
11. Pan, Y., et al., *Mechanisms of transcription factor selectivity.* Trends Genet, 2010. **26**(2): p. 75-83.
12. Zhu, R., et al., *Allosteric histidine switch for regulation of intracellular zinc(II) fluctuation.* Proc Natl Acad Sci U S A, 2017. **114**(52): p. 13661-13666.
13. Lu, S. and J. Zhang, *Designed covalent allosteric modulators: an emerging paradigm in drug discovery.* Drug Discov Today, 2017. **22**(2): p. 447-453.
14. Nussinov, R. and C.-J. Tsai, *Allostery in Disease and in Drug Discovery.* Cell, 2013. **153**(2): p. 293-305.
15. Nussinov, R., et al., *Allosteric post-translational modification codes.* Trends Biochem Sci, 2012. **37**(10): p. 447-55.
16. Patricelli, M.P., et al., *Selective Inhibition of Oncogenic KRAS Output with Small Molecules Targeting the Inactive State.* Cancer discovery, 2016. **6**(3): p. 316-329.
17. Sinha, N. and R. Nussinov, *Point mutations and sequence variability in proteins: redistributions of preexisting populations.* Proc Natl Acad Sci U S A, 2001. **98**(6): p. 3139-44.
18. Strickland, D., K. Moffat, and T.R. Sosnick, *Light-activated DNA binding in a designed allosteric protein.* Proc Natl Acad Sci U S A, 2008. **105**(31): p. 10709-14.
19. Capdevila, D.A., et al., *Entropy redistribution controls allostery in a metalloregulatory protein.* Proceedings of the National Academy of Sciences, 2017. **114**(17): p. 4424.

20. Di Russo, N.V., M.A. Martí, and A.E. Roitberg, *Underlying Thermodynamics of pH-Dependent Allostery.* The Journal of Physical Chemistry B, 2014. **118**(45): p. 12818-12826.
21. Gafurov, B., Y.D. Chen, and J.M. Chalovich, *Ca2+ and ionic strength dependencies of S1-ADP binding to actin-tropomyosin-troponin: regulatory implications.* Biophys J, 2004. **87**(3): p. 1825-35.
22. Buzko, O. and K.M. Shokat, *A kinase sequence database: sequence alignments and family assignment.* Bioinformatics, 2002. **18**(9): p. 1274-5.
23. Yang, J.S., et al., *Rational engineering of enzyme allosteric regulation through sequence evolution analysis.* PLoS Comput Biol, 2012. **8**(7): p. e1002612.
24. Grover, A.K., *Use of allosteric targets in the discovery of safer drugs.* Med Princ Pract, 2013. **22**(5): p. 418-26.
25. Korczynska, M., et al., *Structure-based discovery of selective positive allosteric modulators of antagonists for the M(2) muscarinic acetylcholine receptor.* Proc Natl Acad Sci U S A, 2018. **115**(10): p. E2419-e2428.
26. Nussinov, R. and C.J. Tsai, *The design of covalent allosteric drugs.* Annu Rev Pharmacol Toxicol, 2015. **55**: p. 249-67.
27. Lazareno, S., et al., *Thiochrome enhances acetylcholine affinity at muscarinic M4 receptors: receptor subtype selectivity via cooperativity rather than affinity.* Mol Pharmacol, 2004. **65**(1): p. 257-66.
28. Conn, P.J., A. Christopoulos, and C.W. Lindsley, *Allosteric modulators of GPCRs: a novel approach for the treatment of CNS disorders.* Nat Rev Drug Discov, 2009. **8**(1): p. 41-54.
29. Nussinov, R. and C.J. Tsai, *The different ways through which specificity works in orthosteric and allosteric drugs.* Curr Pharm Des, 2012. **18**(9): p. 1311-6.
30. Conn, P.J., et al., *Opportunities and challenges in the discovery of allosteric modulators of GPCRs for treating CNS disorders.* Nat Rev Drug Discov, 2014. **13**(9): p. 692-708.
31. Szilágyi, A., R. Nussinov, and P. Csermely, *Allo-network drugs: extension of the allosteric drug concept to protein- protein interaction and signaling networks.* Curr Top Med Chem, 2013. **13**(1): p. 64-77.
32. Schelshorn, D., et al., *Lateral allosterism in the glucagon receptor family: glucagon-like peptide 1 induces G-protein-coupled receptor heteromer formation.* Mol Pharmacol, 2012. **81**(3): p. 309-18.
33. Wenthur, C.J., et al., *Drugs for allosteric sites on receptors.* Annu Rev Pharmacol Toxicol, 2014. **54**: p. 165-84.
34. Urwyler, S., *Allosteric modulation of family C G-protein-coupled receptors: from molecular insights to therapeutic perspectives.* Pharmacol Rev, 2011. **63**(1): p. 59-126.
35. van Westen, G.J.P., A. Gaulton, and J.P. Overington, *Chemical, Target, and Bioactive Properties of Allosteric Modulation.* PLOS Computational Biology, 2014. **10**(4): p. e1003559.
36. Kruger, F.A. and J.P. Overington, *Global analysis of small molecule binding to related protein targets.* PLoS Comput Biol, 2012. **8**(1): p. e1002333.
37. Lu, S., W. Huang, and J. Zhang, *Recent computational advances in the identification of allosteric sites in proteins.* Drug Discov Today, 2014. **19**(10): p. 1595-600.
38. Ni, D., S. Lu, and J. Zhang, *Methods Applied for the Allosteric Site Revelation*. 2018: Encyclopedia of Analytical Chemistry.

39. Wagner, J.R., et al., *Emerging Computational Methods for the Rational Discovery of Allosteric Drugs.* Chem Rev, 2016. **116**(11): p. 6370-90.
40. Omer, A. and C.S. Prasad, *Designing allosteric modulators for active conformational state of m-glutamate G-protein coupled receptors.* Bioinformation, 2012. **8**(4): p. 170-4.
41. Song, K., et al., *Improved Method for the Identification and Validation of Allosteric Sites.* J Chem Inf Model, 2017. **57**(9): p. 2358-2363.
42. Li, X., et al., *Toward an understanding of the sequence and structural basis of allosteric proteins.* J Mol Graph Model, 2013. **40**: p. 30-9.
43. Changeux, J.-P., *Allostery and the Monod-Wyman-Changeux Model After 50 Years.* Annual Review of Biophysics, 2012. **41**(1): p. 103-133.
44. Smith, R.D., J. Lu, and H.A. Carlson, *Are there physicochemical differences between allosteric and competitive ligands?* PLoS Comput Biol, 2017. **13**(11): p. e1005813.
45. Chothia, C. and J. Janin, *Principles of protein-protein recognition.* Nature, 1975. **256**(5520): p. 705-8.
46. Gruber, J., et al., *Computational analyses of the surface properties of protein-protein interfaces.* Acta Crystallogr D Biol Crystallogr, 2007. **63**(Pt 1): p. 50-7.
47. De Cesco, S., et al., *Covalent inhibitors design and discovery.* Eur J Med Chem, 2017. **138**: p. 96-114.
48. Xu, Y., et al., *Covalent inhibitors of LgtC: A blueprint for the discovery of non-substrate-like inhibitors for bacterial glycosyltransferases.* Bioorg Med Chem, 2017. **25**(12): p. 3182-3194.
49. Tsai, C.J. and R. Nussinov, *A unified view of "how allostery works".* PLoS Comput Biol, 2014. **10**(2): p. e1003394.
50. Nussinov, R. and C.J. Tsai, *Unraveling structural mechanisms of allosteric drug action.* Trends Pharmacol Sci, 2014. **35**(5): p. 256-64.
51. Engers, D.W. and C.W. Lindsley, *Allosteric modulation of Class C GPCRs: a novel approach for the treatment of CNS disorders.* Drug Discov Today Technol, 2013. **10**(2): p. e269-76.
52. Nussinov, R., C.J. Tsai, and J. Liu, *Principles of allosteric interactions in cell signaling.* J Am Chem Soc, 2014. **136**(51): p. 17692-701.
53. Wang, Q., et al., *Toward understanding the molecular basis for chemical allosteric modulator design.* Journal of Molecular Graphics and Modelling, 2012. **38**: p. 324-333.
54. Jacobsen, S.E., U. Gether, and H. Bräuner-Osborne, *Investigating the molecular mechanism of positive and negative allosteric modulators in the calcium-sensing receptor dimer.* Scientific Reports, 2017. **7**(1): p. 46355.
55. Wold, E.A., et al., *Allosteric Modulation of Class A GPCRs: Targets, Agents, and Emerging Concepts.* Journal of medicinal chemistry, 2019. **62**(1): p. 88-127.
56. Springthorpe, B., et al., *From ATP to AZD6140: the discovery of an orally active reversible P2Y12 receptor antagonist for the prevention of thrombosis.* Bioorg Med Chem Lett, 2007. **17**(21): p. 6013-8.
57. Garcia-Perez, J., et al., *New insights into the mechanisms whereby low molecular weight CCR5 ligands inhibit HIV-1 infection.* J Biol Chem, 2011. **286**(7): p. 4978-90.
58. Waugh, D.J., et al., *Binding, partial agonism, and potentiation of alpha(1)-adrenergic receptor function by benzodiazepines: A potential site of allosteric modulation.* J Pharmacol Exp Ther, 1999. **291**(3): p. 1164-71.

59. Morlock, E.V. and C. Czajkowski, *Different residues in the GABAA receptor benzodiazepine binding pocket mediate benzodiazepine efficacy and binding.* Mol Pharmacol, 2011. **80**(1): p. 14-22.
60. Sigel, E., *Mapping of the benzodiazepine recognition site on GABA(A) receptors.* Curr Top Med Chem, 2002. **2**(8): p. 833-9.
61. Sigel, E. and M.E. Steinmann, *Structure, function, and modulation of GABA(A) receptors.* J Biol Chem, 2012. **287**(48): p. 40224-31.
62. Zhu, S., et al., *Structure of a human synaptic GABA(A) receptor.* Nature, 2018. **559**(7712): p. 67-72.
63. Möhler, H., J.M. Fritschy, and U. Rudolph, *A new benzodiazepine pharmacology.* J Pharmacol Exp Ther, 2002. **300**(1): p. 2-8.
64. Riss, J., et al., *Benzodiazepines in epilepsy: pharmacology and pharmacokinetics.* Acta Neurol Scand, 2008. **118**(2): p. 69-86.
65. Quirk, J.C. and E.S. Nisenbaum, *Multiple molecular determinants for allosteric modulation of alternatively spliced AMPA receptors.* J Neurosci, 2003. **23**(34): p. 10953-62.
66. Desai, M.A., et al., *Cyclothiazide acts at a site on the alpha-amino-3-hydroxy-5-methyl-4-isoxazole propionic acid receptor complex that does not recognize competitive or noncompetitive AMPA receptor antagonists.* J Pharmacol Exp Ther, 1995. **272**(1): p. 38-43.
67. Feng, H.J., et al., *Etomidate produces similar allosteric modulation in α1β3δ and α1β3γ2L GABA(A) receptors.* Br J Pharmacol, 2014. **171**(3): p. 789-98.
68. Vinkers, C.H., et al., *Discriminative stimulus properties of GABAA receptor positive allosteric modulators TPA023, ocinaplon and NG2-73 in rats trained to discriminate chlordiazepoxide or zolpidem.* Eur J Pharmacol, 2011. **668**(1-2): p. 190-3.
69. Richter, G., et al., *The Z-Drugs Zolpidem, Zaleplon, and Eszopiclone Have Varying Actions on Human GABA (A) Receptors Containing γ1, γ2, and γ3 Subunits.* Front Neurosci, 2020. **14**: p. 599812.
70. *Pinpointing the Binding Sites of the Common Anesthetic Propofol in GABA Type A Receptors♦: Multiple Propofol-binding Sites in a γ-Aminobutyric Acid Type A Receptor (GABA(A)R) Identified Using a Photoreactive Propofol Analog.* The Journal of Biological Chemistry, 2014. **289**(40): p. 27469-27469.
71. Liang, Q., et al., *Positive Allosteric Modulation of Kv Channels by Sevoflurane: Insights into the Structural Basis of Inhaled Anesthetic Action.* PLoS One, 2015. **10**(11): p. e0143363.
72. Mapelli, J., et al., *The effects of the general anesthetic sevoflurane on neurotransmission: an experimental and computational study.* Scientific Reports, 2021. **11**(1): p. 4335.
73. Ahmed, A.H. and R.E. Oswald, *Piracetam defines a new binding site for allosteric modulators of alpha-amino-3-hydroxy-5-methyl-4-isoxazole-propionic acid (AMPA) receptors.* Journal of medicinal chemistry, 2010. **53**(5): p. 2197-2203.
74. Quirk, J.C. and E.S. Nisenbaum, *Multiple molecular determinants for allosteric modulation of alternatively spliced AMPA receptors.* The Journal of neuroscience : the official journal of the Society for Neuroscience, 2003. **23**(34): p. 10953-10962.
75. Rogawski, M.A. and T. Hanada, *Preclinical pharmacology of perampanel, a selective non-competitive AMPA receptor antagonist.* Acta Neurol Scand Suppl, 2013(197): p. 19-24.

76. Schoemaker, H., et al., *Allosteric modulation by diltiazem and verapamil of [3H]nitrendipine binding to calcium channel sites in rat brain.* Proc West Pharmacol Soc, 1983. **26**: p. 219-24.
77. Holck, M., W. Fischli, and U. Hengartner, *Effects of temperature and allosteric modulators on [3H] nitrendipine binding: methods for detecting potential Ca2+ channel blockers.* J Recept Res, 1984. **4**(1-6): p. 557-69.
78. Tang, L., et al., *Structural Basis for Diltiazem Block of a Voltage-gated Ca2+ Channel.* Molecular Pharmacology, 2019: p. mol.119.117531.
79. Porzig, H. and C. Becker, *Potential-dependent allosteric modulation of 1,4-dihydropyridine binding by d-(cis)-diltiazem and (+/-)-verapamil in living cardiac cells.* Mol Pharmacol, 1988. **34**(2): p. 172-9.
80. Guzman, J.N., et al., *Systemic isradipine treatment diminishes calcium-dependent mitochondrial oxidant stress.* The Journal of clinical investigation, 2018. **128**(6): p. 2266-2280.
81. Vallés, A.S., et al., *A novel agonist effect on the nicotinic acetylcholine receptor exerted by the anticonvulsive drug Lamotrigine.* Biochimica et Biophysica Acta (BBA) - Biomembranes, 2008. **1778**(10): p. 2395-2404.
82. Twyman, R.E., C.J. Rogers, and R.L. Macdonald, *Differential regulation of gamma-aminobutyric acid receptor channels by diazepam and phenobarbital.* Ann Neurol, 1989. **25**(3): p. 213-20.
83. Krause, R.M., et al., *Ivermectin: a positive allosteric effector of the alpha7 neuronal nicotinic acetylcholine receptor.* Mol Pharmacol, 1998. **53**(2): p. 283-94.
84. Häberle, J., *Role of carglumic acid in the treatment of acute hyperammonemia due to N-acetylglutamate synthase deficiency.* Ther Clin Risk Manag, 2011. **7**: p. 327-32.
85. Gilmartin, A.G., et al., *GSK1120212 (JTP-74057) is an inhibitor of MEK activity and activation with favorable pharmacokinetic properties for sustained in vivo pathway inhibition.* Clin Cancer Res, 2011. **17**(5): p. 989-1000.
86. Chiu, M.I., H. Katz, and V. Berlin, *RAPT1, a mammalian homolog of yeast Tor, interacts with the FKBP12/rapamycin complex.* Proceedings of the National Academy of Sciences of the United States of America, 1994. **91**(26): p. 12574-12578.
87. Chen, J., et al., *Allosteric inhibitor remotely modulates the conformation of the orthestric pockets in mutant IDH2/R140Q.* Sci Rep, 2017. **7**(1): p. 16458.
88. Schauer, G.D., et al., *Mechanism of allosteric inhibition of HIV-1 reverse transcriptase revealed by single-molecule and ensemble fluorescence.* Nucleic acids research, 2014. **42**(18): p. 11687-11696.
89. Artsimovitch, I., et al., *Allosteric modulation of the RNA polymerase catalytic reaction is an essential component of transcription control by rifamycins.* Cell, 2005. **122**(3): p. 351-63.
90. Changeux, J.-P. and A. Christopoulos, *Allosteric Modulation as a Unifying Mechanism for Receptor Function and Regulation.* Cell, 2016. **166**(5): p. 1084-1102.
91. Chiarini, F., et al., *A combination of temsirolimus, an allosteric mTOR inhibitor, with clofarabine as a new therapeutic option for patients with acute myeloid leukemia.* Oncotarget, 2012. **3**(12): p. 1615-1628.
92. Yang, L., et al., *Thrombomodulin enhances the reactivity of thrombin with protein C inhibitor by providing both a binding site for the serpin and allosterically modulating the activity of thrombin.* J Biol Chem, 2003. **278**(39): p. 37465-70.

93. Cheng, Y. and H. Tian, *Current Development Status of MEK Inhibitors.* Molecules (Basel, Switzerland), 2017. **22**(10): p. 1551.
94. Cho, H.S., et al., *Structure of the extracellular region of HER2 alone and in complex with the Herceptin Fab.* Nature, 2003. **421**(6924): p. 756-60.
95. Franklin, M.C., et al., *Insights into ErbB signaling from the structure of the ErbB2-pertuzumab complex.* Cancer Cell, 2004. **5**(4): p. 317-28.
96. Wick, J.Y., *The history of benzodiazepines.* Consult Pharm, 2013. **28**(9): p. 538-48.
97. Skerritt, J.H. and G.A. Johnston, *Enhancement of GABA binding by benzodiazepines and related anxiolytics.* Eur J Pharmacol, 1983. **89**(3-4): p. 193-8.
98. Study, R.E. and J.L. Barker, *Cellular mechanisms of benzodiazepine action.* Jama, 1982. **247**(15): p. 2147-51.
99. Olsen, R.W., et al., *Barbiturate and benzodiazepine modulation of GABA receptor binding and function.* Life Sci, 1986. **39**(21): p. 1969-76.
100. de Francisco, A.L., *Cinacalcet HCl: a novel therapeutic for hyperparathyroidism.* Expert Opin Pharmacother, 2005. **6**(3): p. 441-52.
101. Moe, S.M., et al., *Long-term treatment of secondary hyperparathyroidism with the calcimimetic cinacalcet HCl.* Nephrol Dial Transplant, 2005. **20**(10): p. 2186-93.
102. Cunningham, J., *Management of secondary hyperparathyroidism.* Ther Apher Dial, 2005. **9 Suppl 1**: p. S35-40.
103. Eriguchi, R., et al., *Successful treatment of inoperable recurrent secondary hyperparathyroidism with cinacalcet HCl.* NDT Plus, 2008. **1**(4): p. 218-220.
104. Meola, M., I. Petrucci, and G. Barsotti, *Long-term treatment with cinacalcet and conventional therapy reduces parathyroid hyperplasia in severe secondary hyperparathyroidism.* Nephrol Dial Transplant, 2009. **24**(3): p. 982-9.
105. Goodsell, D.S., et al., *RCSB Protein Data Bank: Enabling biomedical research and drug discovery.* Protein Sci, 2020. **29**(1): p. 52-65.
106. Huang, Z., et al., *ASD: a comprehensive database of allosteric proteins and modulators.* Nucleic Acids Res, 2011. **39**(Database issue): p. D663-9.
107. Liu, X., et al., *Mechanism of intracellular allosteric β(2)AR antagonist revealed by X-ray crystal structure.* Nature, 2017. **548**(7668): p. 480-484.
108. Feng, Z., et al., *Allosteric Binding Site and Activation Mechanism of Class C G-Protein Coupled Receptors: Metabotropic Glutamate Receptor Family.* AAPS J., 2015. **17**(3): p. 737-753.
109. Hou, T., et al., *Integrated multi-class classification and prediction of GPCR allosteric modulators by machine learning intelligence.* Biomolecules, 2021. **11**(6): p. 870.
110. Bian, Y., et al., *Integrated In Silico Fragment-Based Drug Design: Case Study with Allosteric Modulators on Metabotropic Glutamate Receptor 5.* AAPS J., 2017. **19**(4): p. 1235-1248.
111. Feng, Z., et al., *Modeling, Molecular Dynamics Simulation, and Mutation Validation for Structure of Cannabinoid Receptor 2 Based on Known Crystal Structures of GPCRs.* J. Chem. Inf. Model., 2014. **54**(9): p. 2483-2499.
112. Bian, Y., et al., *Prediction of Orthosteric and Allosteric Regulations on Cannabinoid Receptors Using Supervised Machine Learning Classifiers.* Mol. Pharmaceutics, 2019. **16**(6): p. 2605-2615.
113. Feng, Z., et al., *Computational Advances for the Development of Allosteric Modulators and Bitopic Ligands in G Protein-Coupled Receptors.* Aaps j, 2015. **17**(5): p. 1080-95.

114. Feng, Z., et al., *Binding Characterization of GPCRs-Modulator by Molecular Complex Characterizing System (MCCS).* ACS Chem Neurosci, 2020.
115. Chen, M., et al., *MCCS, a novel characterization method for protein-ligand complex.* Brief Bioinform, 2021. **22**(4).
116. Molinoff, P.B., *Alpha- and beta-adrenergic receptor subtypes properties, distribution and regulation.* Drugs, 1984. **28 Suppl 2**: p. 1-15.
117. Triposkiadis, F., et al., *The sympathetic nervous system in heart failure physiology, pathophysiology, and clinical implications.* J Am Coll Cardiol, 2009. **54**(19): p. 1747-62.
118. De Backer, I., et al., *Insights into the role of neuronal glucokinase.* Am J Physiol Endocrinol Metab, 2016. **311**(1): p. E42-55.
119. Iynedjian, P.B., *Molecular physiology of mammalian glucokinase.* Cellular and molecular life sciences : CMLS, 2009. **66**(1): p. 27-42.
120. Platt, S.R., *The role of glutamate in central nervous system health and disease--a review.* Vet J, 2007. **173**(2): p. 278-86.
121. Limatola, C., *Neurotrophic effects of AMPA.* Cerebellum, 2004. **3**(1): p. 2-10.
122. Zhou, Q. and M. Sheng, *NMDA receptors in nervous system diseases.* Neuropharmacology, 2013. **74**: p. 69-75.
123. Zanetti, L., et al., *Presynaptic AMPA Receptors in Health and Disease.* Cells, 2021. **10**(9).
124. Berman, H.M., et al., *The Protein Data Bank.* Nucleic Acids Res, 2000. **28**(1): p. 235-42.
125. Pettersen, E.F., et al., *UCSF Chimera--a visualization system for exploratory research and analysis.* J Comput Chem, 2004. **25**(13): p. 1605-12.
126. Shapovalov, M.V. and R.L. Dunbrack, Jr., *A smoothed backbone-dependent rotamer library for proteins derived from adaptive kernel density estimates and regressions.* Structure, 2011. **19**(6): p. 844-58.
127. Pedretti, A., L. Villa, and G. Vistoli, *VEGA – An open platform to develop chemo-bio-informatics applications, using plug-in architecture and script programming.* Journal of Computer-Aided Molecular Design, 2004. **18**(3): p. 167-173.
128. Olsson, M.H.M., et al., *PROPKA3: Consistent Treatment of Internal and Surface Residues in Empirical pKa Predictions.* Journal of Chemical Theory and Computation, 2011. **7**(2): p. 525-537.
129. Søndergaard, C.R., et al., *Improved Treatment of Ligands and Coupling Effects in Empirical Calculation and Rationalization of pKa Values.* Journal of Chemical Theory and Computation, 2011. **7**(7): p. 2284-2295.
130. Li, H., K. Leung, and M.-H. Wong, *Idock: A multithreaded virtual screening tool for flexible ligand docking.* 2012 IEEE Symposium on Computational Intelligence in Bioinformatics and Computational Biology (CIBCB), 2012.
131. Wan, S., et al., *Rapid, accurate, precise and reproducible ligand–protein binding free energy prediction.* Interface Focus, 2020. **10**(6): p. 20200007.
132. Hall, R., T. Dixon, and A. Dickson, *On Calculating Free Energy Differences Using Ensembles of Transition Paths.* Frontiers in Molecular Biosciences, 2020. **7**.
133. Trott, O. and A.J. Olson, *AutoDock Vina: improving the speed and accuracy of docking with a new scoring function, efficient optimization, and multithreading.* J Comput Chem, 2010. **31**(2): p. 455-61.
134. Morris, G.M., et al., *AutoDock4 and AutoDockTools4: Automated docking with selective receptor flexibility.* Journal of computational chemistry, 2009. **30**(16): p. 2785-2791.

135. Jorgensen, W.L., et al., *Comparison of simple potential functions for simulating liquid water.* The Journal of Chemical Physics, 1983. **79**(2): p. 926-935.
136. Jo, S., T. Kim, and W. Im, *Automated builder and database of protein/membrane complexes for molecular dynamics simulations.* PLoS One, 2007. **2**(9): p. e880.
137. Maier, J.A., et al., *ff14SB: Improving the Accuracy of Protein Side Chain and Backbone Parameters from ff99SB.* J Chem Theory Comput, 2015. **11**(8): p. 3696-713.
138. Jakalian, A., D.B. Jack, and C.I. Bayly, *Fast, efficient generation of high-quality atomic charges. AM1-BCC model: II. Parameterization and validation.* J Comput Chem, 2002. **23**(16): p. 1623-41.
139. Wang, J., et al., *Development and testing of a general amber force field.* J Comput Chem, 2004. **25**(9): p. 1157-74.
140. Götz, A.W., et al., *Routine Microsecond Molecular Dynamics Simulations with AMBER on GPUs. 1. Generalized Born.* J Chem Theory Comput, 2012. **8**(5): p. 1542-1555.
141. Salomon-Ferrer, R., et al., *Routine Microsecond Molecular Dynamics Simulations with AMBER on GPUs. 2. Explicit Solvent Particle Mesh Ewald.* J Chem Theory Comput, 2013. **9**(9): p. 3878-88.
142. Case D.A., B.R.M., Cerutti D.S., Cheatham T.E., III, Darden T.A., Duke R.E. et al. *AMBER 2016.* 2016.
143. Loncharich, R.J., B.R. Brooks, and R.W. Pastor, *Langevin dynamics of peptides: The frictional dependence of isomerization rates of N-acetylalanyl-N′-methylamide.* Biopolymers, 1992. **32**(5): p. 523-535.
144. Izaguirre, J.A., et al., *Langevin stabilization of molecular dynamics.* The Journal of Chemical Physics, 2001. **114**(5): p. 2090-2098.
145. Darden, T., D. York, and L. Pedersen, *Particle mesh Ewald: An N·log(N) method for Ewald sums in large systems.* The Journal of Chemical Physics, 1993. **98**(12): p. 10089-10092.
146. Essmann, U., et al., *A smooth particle mesh Ewald method.* The Journal of Chemical Physics, 1995. **103**(19): p. 8577-8593.
147. Ryckaert, J.-P., G. Ciccotti, and H.J.C. Berendsen, *Numerical integration of the cartesian equations of motion of a system with constraints: molecular dynamics of n-alkanes.* Journal of Computational Physics, 1977. **23**(3): p. 327-341.
148. Feng, Z., et al., *Binding Characterization of GPCRs-Modulator by Molecular Complex Characterizing System (MCCS).* ACS Chem Neurosci, 2020. **11**(20): p. 3333-3345.
149. Feng, Z., et al., *MCCS: a novel recognition pattern-based method for fast track discovery of anti-SARS-CoV-2 drugs.* Brief Bioinform, 2021. **22**(2): p. 946-962.
150. Cheng, J., et al., *Binding Characterization of Agonists and Antagonists by MCCS: A Case Study from Adenosine A(2A) Receptor.* ACS Chem Neurosci, 2021. **12**(9): p. 1606-1620.
151. Kruse, A.C., et al., *Activation and allosteric modulation of a muscarinic acetylcholine receptor.* Nature, 2013. **504**(7478): p. 101-6.
152. Wieland, K., et al., *Involvement of Asn-293 in stereospecific agonist recognition and in activation of the beta 2-adrenergic receptor.* Proc Natl Acad Sci U S A, 1996. **93**(17): p. 9276-81.
153. Hanson, M.A., et al., *A specific cholesterol binding site is established by the 2.8 A structure of the human beta2-adrenergic receptor.* Structure, 2008. **16**(6): p. 897-905.
154. Sum, C.S., et al., *Identification of Residues Important for Agonist Recognition and Activation in GPR40*.* Journal of Biological Chemistry, 2007. **282**(40): p. 29248-29255.

155. Kornev, A.P., et al., *Surface comparison of active and inactive protein kinases identifies a conserved activation mechanism.* Proc Natl Acad Sci U S A, 2006. **103**(47): p. 17783-8.
156. Biondi, R.M., et al., *High resolution crystal structure of the human PDK1 catalytic domain defines the regulatory phosphopeptide docking site.* Embo j, 2002. **21**(16): p. 4219-28.
157. Komander, D., et al., *Role of T-loop phosphorylation in PDK1 activation, stability, and substrate binding.* J Biol Chem, 2005. **280**(19): p. 18797-802.
158. Busschots, K., et al., *Substrate-selective inhibition of protein kinase PDK1 by small compounds that bind to the PIF-pocket allosteric docking site.* Chem Biol, 2012. **19**(9): p. 1152-63.
159. Pastor-Flores, D., et al., *PIF-Pocket as a Target for C. albicans Pkh Selective Inhibitors.* ACS Chemical Biology, 2013. **8**(10): p. 2283-2292.
160. Wu, P.K. and J.I. Park, *MEK1/2 Inhibitors: Molecular Activity and Resistance Mechanisms.* Semin Oncol, 2015. **42**(6): p. 849-62.
161. Harding, A., et al., *Mechanism of Mitosis-specific Activation of MEK1*.* Journal of Biological Chemistry, 2003. **278**(19): p. 16747-16754.
162. Fischmann, T.O., et al., *Crystal Structures of MEK1 Binary and Ternary Complexes with Nucleotides and Inhibitors.* Biochemistry, 2009. **48**(12): p. 2661-2674.
163. Ohren, J.F., et al., *Structures of human MAP kinase kinase 1 (MEK1) and MEK2 describe novel noncompetitive kinase inhibition.* Nat Struct Mol Biol, 2004. **11**(12): p. 1192-7.
164. Spicer, J.A., et al., *4-anilino-5-carboxamido-2-pyridone derivatives as noncompetitive inhibitors of mitogen-activated protein kinase kinase.* J Med Chem, 2007. **50**(21): p. 5090-102.
165. Warmus, J.S., et al., *2-Alkylamino- and alkoxy-substituted 2-amino-1,3,4-oxadiazoles-O-Alkyl benzohydroxamate esters replacements retain the desired inhibition and selectivity against MEK (MAP ERK kinase).* Bioorg Med Chem Lett, 2008. **18**(23): p. 6171-4.
166. Tecle, H., et al., *Beyond the MEK-pocket: can current MEK kinase inhibitors be utilized to synthesize novel type III NCKIs? Does the MEK-pocket exist in kinases other than MEK?* Bioorg Med Chem Lett, 2009. **19**(1): p. 226-9.
167. Iverson, C., et al., *RDEA119/BAY 869766: a potent, selective, allosteric inhibitor of MEK1/2 for the treatment of cancer.* Cancer Res, 2009. **69**(17): p. 6839-47.
168. Dong, Q., et al., *Discovery of TAK-733, a potent and selective MEK allosteric site inhibitor for the treatment of cancer.* Bioorg Med Chem Lett, 2011. **21**(5): p. 1315-9.
169. Wallace, M.B., et al., *Structure-based design and synthesis of pyrrole derivatives as MEK inhibitors.* Bioorg Med Chem Lett, 2010. **20**(14): p. 4156-8.
170. Gloyn, A.L., et al., *Insights into the biochemical and genetic basis of glucokinase activation from naturally occurring hypoglycemia mutations.* Diabetes, 2003. **52**(9): p. 2433-40.
171. Heredia, V.V., et al., *Biochemical basis of glucokinase activation and the regulation by glucokinase regulatory protein in naturally occurring mutations.* J Biol Chem, 2006. **281**(52): p. 40201-7.
172. Martínez, R., et al., *Heterogeneity in phenotype of hyperinsulinism caused by activating glucokinase mutations: a novel mutation and its functional characterization.* Clin Endocrinol (Oxf), 2017. **86**(6): p. 778-783.
173. Sun, Q., et al., *Discovery of small molecules that bind to K-Ras and inhibit Sos-mediated activation.* Angew Chem Int Ed Engl, 2012. **51**(25): p. 6140-3.

174. Maurer, T., et al., *Small-molecule ligands bind to a distinct pocket in Ras and inhibit SOS-mediated nucleotide exchange activity.* Proc Natl Acad Sci U S A, 2012. **109**(14): p. 5299-304.
175. Li, M., et al., *Novel inhibitors complexed with glutamate dehydrogenase: allosteric regulation by control of protein dynamics.* J Biol Chem, 2009. **284**(34): p. 22988-3000.
176. Salussolia, C.L., et al., *Arrangement of subunits in functional NMDA receptors.* The Journal of neuroscience : the official journal of the Society for Neuroscience, 2011. **31**(31): p. 11295-11304.
177. Guo, H., et al., *A NMDA-receptor calcium influx assay sensitive to stimulation by glutamate and glycine/D-serine.* Sci Rep, 2017. **7**(1): p. 11608.
178. Bonaccorso, C., et al., *Glutamate binding-site ligands of NMDA receptors.* Curr Med Chem, 2011. **18**(36): p. 5483-506.
179. Hackos, D.H., et al., *Positive Allosteric Modulators of GluN2A-Containing NMDARs with Distinct Modes of Action and Impacts on Circuit Function.* Neuron, 2016. **89**(5): p. 983-99.
180. Valant, C., et al., *A novel mechanism of G protein-coupled receptor functional selectivity. Muscarinic partial agonist McN-A-343 as a bitopic orthosteric/allosteric ligand.* J Biol Chem, 2008. **283**(43): p. 29312-21.
181. Gregory, K.J., et al., *Identification of orthosteric and allosteric site mutations in M2 muscarinic acetylcholine receptors that contribute to ligand-selective signaling bias.* J Biol Chem, 2010. **285**(10): p. 7459-74.